Metastable Argon Atoms and the Portable Rydberg Generator: or, How I Learned To Stop Worrying and Love Excited Atoms

by

Joshua Houston Gurian
Class of 2004

A thesis submitted to the
faculty of Wesleyan University
in partial fulfillment of the requirements for the
Degree of Bachelor of Arts
with Departmental Honors in Physics

Abstract

The purpose of this thesis is twofold. I first aim to give an overview of Stark recurrence spectroscopy of Rydberg atoms suitable for an undergraduate interested in experimental research in the Morgan Lab. In the second part of the thesis a new apparatus for metastable production and Stark recurrence spectroscopy is introduced, known as the Portable Rydberg Generator. Various methods for metastable production are discussed and compared from an experimental viewpoint. Finally, initial experimental data of metastable argon from this new apparatus is presented.

Acknowledgements

They say it takes a village to raise a child, and this thesis has been no exception. This experiment never would have materialized from paper if not for the hard work and support of David Boule, Tom Castelli, Bruce Strickland, Dick Widlansky, Vacek Miglus, Mirek Koziol, and Anna Milardo. They work magic.

There is also a long list of people who have really gone out of their way to foster my physics education in the lab. I'm greatly indebted to Heric Flores-Rueda, Len Keeler, David Wright, Jon Lambert, and Thomas Clausen. They have all been great mentors and kind friends.

I would have lost my sanity in the lab if were not for the good times with the esteemed Council of Elders. Intown 21, 84 High, 76 Lawn, and 42 Miles. Hilarity ensues. I have been incredibly lucky to have Marcus Van Lier - Walqui as my fellow lab-monkey. As the other half of the atomic duo, he's been a superb labmate and a true friend.

My parents have been incredibly understanding and encouraging, even when they've said to me, "We don't understand what it is that you're doing, but we're glad you're enjoying it."

And the person who started me on this whole adventure, Professor Tom Morgan.

Contents

Abstract **1**

Acknowledgements **2**

Table of Contents **3**

List of Figures **5**

1 Introduction **8**

1.1 Motivation for Study 8

1.2 Introduction to Rydberg Atoms in Stark Fields 9

1.2.1 Hydrogen 9

1.2.2 Multi-electron Atoms 19

1.3 Previous Research 20

2 Methodologies of Spectroscopy **22**

2.1 Absorption Spectra 22

2.2 Fourier Transforms 24

2.3 Recurrence Spectra 26

2.4 Closed Orbit Theory 26

3 The Portable Rydberg Generator 29

3.1 Overview of Design 29

3.2 Metastable States 32

3.2.1 Metastable Hydrogen 32

3.2.2 Multi-Electron Metastable States 35

3.2.3 Methods of Metastable Creation 35

3.3 Electron Sources 37

3.3.1 HeatWave Labs Source 37

3.3.2 Southwest Vacuum Devices Source 38

3.4 Operating Parameters 38

4 Experimental Data and Analysis 42

5 Conclusion and Future Work 46

Appendices

A Stark Frequency Derivation 48

B Hamiltonian Scaling Derivation 53

C Southwest Vacuum Devices Cathode Installation 55

D Properties of Hydrogenic Ellipses 57

E Pictures of the Portable Rydberg Generator 58

Bibliography 61

Index 68

List of Figures

1.1 Diagram of a Bohr atom, a negatively charged electron of mass m revolving around an infinitely massive nucleus at distance r . . 9

1.2 Illustration of $\vec{A}$, the Runge-Lenz vector, for an elliptical orbit around focus F. 13

1.3 Comparison of (a) Coulomb potential and (b) Coulomb potential with a linear Stark term 15

1.4 First order Stark shift for hydrogen for $n = 15$ to $n = 20$ generated by Eq. (1.27) 16

1.5 Parabolic coordinate system. Lines of constant ξ approach $-\infty$, lines of constant η approach ∞. Rotation through ϕ about the z-axis from 0 to 2π. 18

1.6 Comparison between first and second order Stark shifts for H, $n = 15$, $m = 0$. The dashed lines are the first order shift, the solid lines are the second order shift. 19

1.7 Example of avoided crossings. Stark Rydberg sodium absorption calculation from [57]. 21

2.1 Absorption spectra of $\epsilon = -2.7$, $m = 0$, triplet state of helium, taken by Len Keeler in the Morgan Lab on July 6th, 1997 and August 8th, 1997 [32]. 24
2.2 A plot of Eq. (2.6) 25
2.3 Fourier transform of Eq. (2.6). 25
2.4 Recurrence spectra of Fig. 2.1 taken by Len Keeler in the Morgan Lab [32] 27

3.1 Diagram of PRG 30
3.2 End-cup assembly (Side View) 31
3.3 End-cup assembly (Top View) 31
3.4 Diagram of charged particle sweepers (Side View) 32
3.5 Diagram of charged particle sweepers (Top View) 33
3.6 Decay routes by spontaneous emission of the first four energy levels of hydrogen governed by dipole selection rules. 34
3.7 Diagram of HeatWave TB-198 standard series barium tungsten dispenser cathode 37
3.8 PRG electron source (Side and Exploded Top View) (SW-Vacuum Device Configuration) 39
3.9 Southwest Vacuum Devices $C-14$ cathode diagram 40
3.10 Electron source output current (A) of Southwest Vacuum Devices source as a function of acceleration voltage (V). Electron Source heaters were at 12 V, drawing $\sim$2 A. 41

4.1 Experimental argon data illustrating production of metastables by HeatWave source. Plot of normalized end cup current (arb. units) as a function of electron acceleration voltage(volts)(07/09/03). . . 42

4.2 Experimental argon data illustrating production of metastables by Southwest Vacuum Devices source. Plot of normalized end cup current (arb. units) as a function of electron acceleration voltage(volts)(1/23/04). 43

4.3 Comparison of experimental argon metastable data from Fig. 4.1 and Fig. 4.2. 44

4.4 Comparison of experimental argon data and known apparent electron impact excitation cross sections (arb. units) as a function of electron energy (volts). Cross section data taken from [6, 45]. . . . 45

E.1 View of metastable source from the Portable Rydberg Generator (Southwest Vacuum Devices cathodes) 58

E.2 Wide view of the Portable Rydberg Generator 59

E.3 Side view of the Portable Rydberg Generator 60

Chapter 1

Introduction

1.1 Motivation for Study

Highly excited atoms in external perturbations have long been a subject of interest in atomic physics. These highly excited atoms, known as Rydberg atoms, straddle an interesting place in physics. They represent a quantum mechanical system extended into a classical domain. One of the driving purposes of this research has been to try to coalesce these two mechanical formulations. Many of these systems also exhibit the unique property of being classical chaotic, while still being solvable in a quantum mechanical regime. This has become known as "quantum chaos" and is a motivating interest in these systems [30].

The study of Rydberg atoms in static external electric fields, or Stark fields, has become a extremely interesting problem in physics. Even small deviations from a Coulomb potential lead to notable changes in the physics of these Rydberg atoms. Although Rydberg systems have been heavily studied since the 1970s, the application of recurrence spectroscopy to Rydberg systems is a relatively

new innovation [18]. The Nobel gases, with a single electron excited out of the valence shell, provide a complex and interesting system for study. In this thesis we first look to lay a foundation for investigating Rydberg atoms in Stark fields.

1.2 Introduction to Rydberg Atoms in Stark Fields

1.2.1 Hydrogen

Hydrogen, with a single proton and a single electron, clearly represents the simplest classical or quantum mechanical atomic model. Theoretical models of hydrogen can therefore provide a comparison for more complex atoms and yield insight into experimental data.

Semi-Classical Hydrogen

The qualitative classical picture of the Rydberg atom is similar to Keplerian planetary motion. We can quantitatively investigate the classical model of hydrogen by first looking at the Bohr model of the atom.

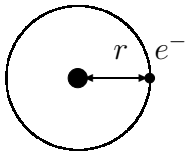

Figure 1.1: Diagram of a Bohr atom, a negatively charged electron of mass m revolving around an infinitely massive nucleus at distance r

First developed by Bohr in 1913, his theory placed a negative electron in a cir-

cular orbit about a stationary positive nucleus of infinite mass (see Fig 1.1) [18]. Bohr himself made the assumption that the angular momentum in the atom was quantized in units of $\hbar$. In order to align his theory with experimental results, Bohr also postulated that the atom did not radiate energy continuously, but only made transitions between states of well defined energies. The angular force on the electron,

$$\frac{mv^2}{r} \tag{1.1}$$

can be equated to the attractive force between the proton and electron,

$$\frac{e^2}{4\pi\epsilon_0 r^2}. \tag{1.2}$$

The angular momentum can be quantized as,

$$mvr = n\hbar \tag{1.3}$$

leading to an expression of the orbital radius of the electron as,

$$r = \frac{4\pi\epsilon_0\hbar^2 n^2}{e^2 m} \tag{1.4}$$

which notably scales as n^2.

We can justify the analogy of the electron being in a Kepler orbit by comparing the orbital radius to the de Broglie wavelength of the electron. For an $n = 15$ excited atom, by Eq. (1.4), our orbital radius is around 119Å. We can compare this distance to the wavelength of the electron, given by the de Broglie formula,

$$p = \frac{h}{\lambda} \tag{1.5}$$

This puts the de Broglie wavelength at 5.6Å, or 0.047 of the electron orbital radius. The de Broglie wavelength is so small compared to the orbital radius

that we can view this highly excited system as a independent particle very far from the nucleus, much akin to a Keplerian system. We can consider the electron in a classical regime when it is far from the nucleus, and no longer as a quantum system.

If the energy of the electron is written as the sum of the kinetic and Coulombic potential energies, where

$$T = \frac{1}{2}mv^2 \tag{1.6a}$$

$$U = -\frac{e^2}{4\pi\epsilon_0 r} \tag{1.6b}$$

We can then write the energy as,

$$E = -\frac{e^4 m}{8\pi\epsilon_0 n^2 \hbar^2} \tag{1.7}$$

clearly scaling as $1/n^2$. This equation is known as the Rydberg energy equation.

We can now further investigate the first order classical energy shift of the electron in an electric field by examining the time averaged permanent dipole moment of hydrogen. It can be noted that any particle in a central field potential has its motion limited to a plane, which we can take to be in polar coordinates [22]. We can begin by writing down the total energy of the system,

$$E = 1/2m\dot{r}^2 + 1/2mr^2\dot{\phi}^2 + U(r) \tag{1.8}$$

The angular kinetic energy can be expressed in terms of the angular momentum by noting that

$$l = mr^2\dot{\phi} \tag{1.9}$$

and therefore

$$E = 1/2m\dot{r}^2 + 1/2\frac{l^2}{mr^2} + U(r) \tag{1.10}$$

By manipulating this equation we can write,

$$\dot{r} = \sqrt{\frac{2}{m}(E - U(r)) - \frac{l^2}{m^2 r^2}} = \frac{dr}{dt} \tag{1.11}$$

or rather,

$$dt = \frac{dr}{\sqrt{\frac{2}{m}(E - U(r)) - \frac{l^2}{m^2 r^2}}} \tag{1.12}$$

Substituting Eq. (1.9), the above equation can be written as

$$d\phi = \frac{\frac{l}{mr^2 dr}}{\sqrt{\frac{2}{m}(E - U(r)) - \frac{l^2}{m^2 r^2}}} \tag{1.13}$$

Now is an opportune moment to introduce atomic units (au) in an attempt to simplify our equations [9]:

$$m_e = 1 \tag{1.14a}$$

$$a_0 = 1 \tag{1.14b}$$

$$e = 1 \tag{1.14c}$$

$$\hbar = 1 \tag{1.14d}$$

$$6.5761 \times 10^6 GHz = 1 \tag{1.14e}$$

$$5.137 \times 10^9 V/cm = 1 \tag{1.14f}$$

One should note that Eq. (1.7), our familiar Rydberg energy formula, now becomes,

$$E = \frac{-1}{2n^2} \tag{1.15}$$

Applying Eq. (1.6b) to Eq. (1.13) and integrating both sides yields

$$\phi = cos^{-1} \frac{l/r - m/l}{\sqrt{2mE + \frac{m^2}{l^2}}} \tag{1.16}$$

As Landau and Lifshitz note [40], the eccentricity of the classical orbit can be written as

$$\epsilon = \sqrt{1 + \frac{2El^2}{m}} \tag{1.17}$$

We can now apply Eq. (1.14) and Eq. (1.17) to Eq. (1.16) and write our equation of motion as

$$l^2/r = 1 + \epsilon cos\phi, \tag{1.18}$$

an ellipse with one focus at the origin.

We can further investigate the classical hydrogen atom by defining the Runge-Lenz vector,

$$\vec{A} = \vec{p} \times \vec{L} - \hat{r} \tag{1.19}$$

It can be shown that the Lenz vector is a constant of motion in Coulombic and gravitational fields, yet $\frac{d\vec{A}}{dt} \neq 0$ when the potential deviates from $1/r$.

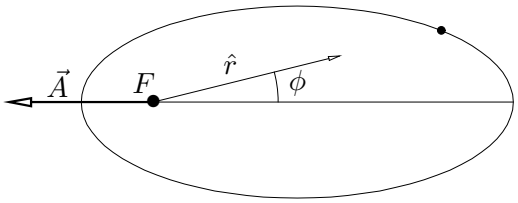

Figure 1.2: Illustration of $\vec{A}$, the Runge-Lenz vector, for an elliptical orbit around focus F.

We can now write the average dipole moment of the atom, $\vec{d}$, as pointing in the direction of the pericenter, equivalent to the direction of $\vec{A}$,

$$< \vec{d} >=< rcos\phi > (\vec{A}/|\vec{A}|) \tag{1.20}$$

We can integrate over a period of motion to find the magnitude of the dipole moment,

$$| < \vec{d} > | = \frac{1}{\tau} \int_0^\tau rcos\phi dt = \frac{1}{\tau} \int_0^\tau rcos\phi \frac{1}{\dot{\phi}} d\phi \tag{1.21}$$

By applying Eq. (1.9), and substituting Eq. (1.18) we can rewrite this integral as

$$| < \vec{d} > | = \frac{l^5}{2\pi n^3} \int_{-\pi}^{\pi} \frac{cos\phi d\phi}{(1 + \epsilon cos\phi)^3} \tag{1.22}$$

noting that

$$\tau = 2\pi n^3 \tag{1.23}$$

We can now evaluate the integral Eq. (1.22) as

$$| < \vec{d} > | = \frac{3}{2} n^2 \epsilon \tag{1.24}$$

As Hezel et al note [27], the magnitude of the Runge-Lenz vector is equal to the eccentricity of the orbit, and therefore

$$< \vec{d} >= \frac{3}{2} n^2 \vec{A} \tag{1.25}$$

The energy of a dipole in an electric field $\vec{F}$ is simply

$$E = -\vec{d} \cdot \vec{F} \tag{1.26}$$

The energy shift from an electric field (Fig. 1.4) in the z-direction for a hydrogen atom is then given by

$$\Delta E = -\frac{3}{2} n^2 A_z F \tag{1.27}$$

We can further investigate the classical dynamics of hydrogen with the Runge-Lenz vector, beginning with Hamilton's equations,

$$\dot{p} = -\vec{\nabla}_r H \tag{1.28a}$$

$$\dot{r} = \vec{\nabla}_p H \tag{1.28b}$$

As Hezel et al show (a full, more explicit derivation is found in Appendix A), we can generate from Eqs. (1.28) a pair of uncoupled equations for the Lenz vector

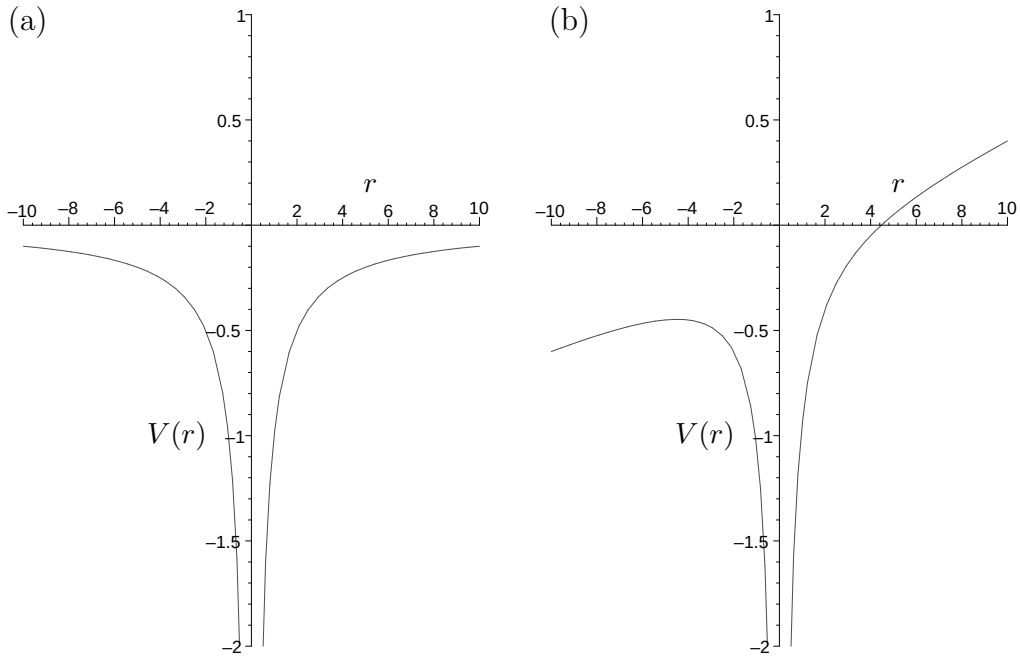

Figure 1.3: Comparison of (a) Coulomb potential and (b) Coulomb potential with a linear Stark term

and angular momentum of classical hydrogen [27]:

$$A_x(t)^2 + A_y(t)^2 = A_{x0}^2 \cos^2(\omega_s t) + A_{y0}^2 \sin^2(\omega_s t) \tag{1.29a}$$

$$L_x(t)^2 + L_y(t)^2 = L_{x0}^2 \cos^2(\omega_s t) + L_{y0}^2 \sin^2(\omega_s t) \tag{1.29b}$$

$$\text{where} \qquad \omega_s = \frac{3}{2} nF \tag{1.29c}$$

ω_s is known as the Stark frequency [27]. Eqs. (1.29) describe an orbital ellipse that precesses at frequency ω_s about the origin while the orbital plane precesses about the axis of the electric field at the same frequency ω_s. Our total system energy stays constant and so the orbital semimajor axis must also stay constant. The orbital precession is consequently exhibited in changes in the length of the semiminor axis (see Appendix D for diagram of elliptical definitions).

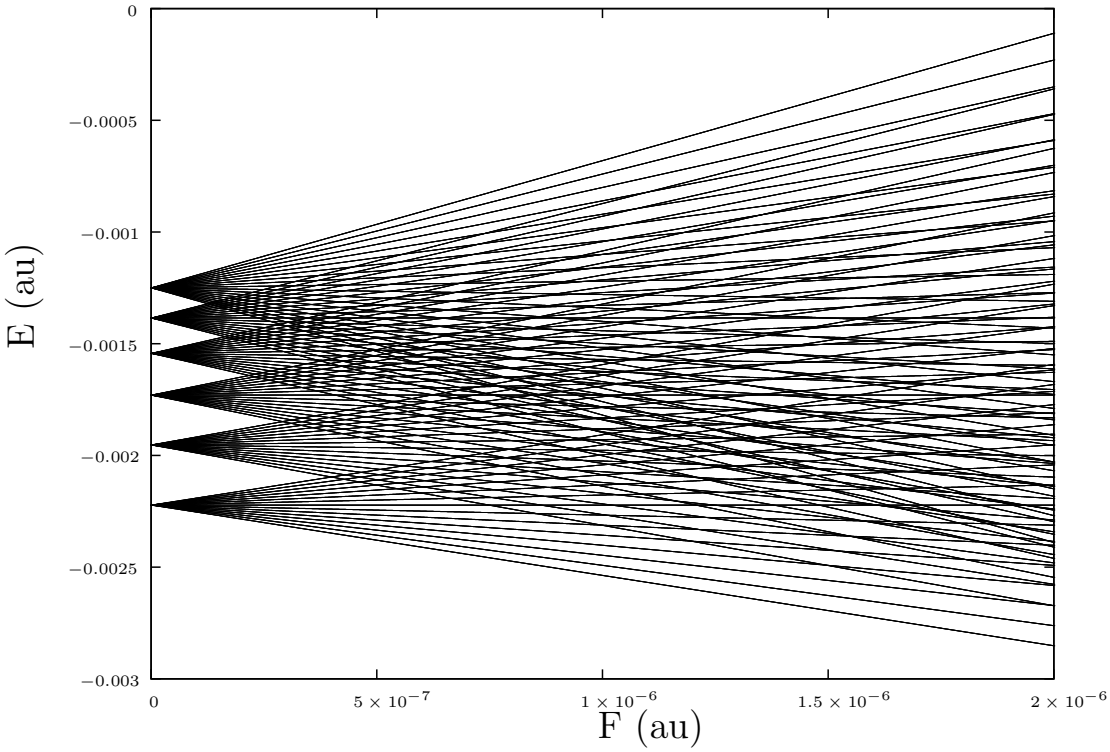

Figure 1.4: First order Stark shift for hydrogen for $n = 15$ to $n = 20$ generated by Eq. (1.27)

Quantum Mechanical Hydrogen

We can also approach hydrogen from a quantum mechanical perspective. For the zero field case, we can begin with the simple three dimensional Schrödinger equation,

$$\hat{H}\Psi = E\Psi \tag{1.30}$$

Using the same Coulombic potential as in Eq. (1.6b), we can easily find the energies of this system to be equal to Eq. (1.7), therefore in agreement with Bohr's model of the atom [23].

Separation of the Schrödinger equation in spherical coordinates using the operators $\hat{H}$, $\hat{L^2}$, and $\hat{L_z}$ yields the valid quantum numbers n, l, and m - the

familiar principle, angular, and magnetic quantum numbers, respectively. However, when an electric field is applied to the atom, and therefore an additional term added to the potential, the Hamiltonian is no longer separable in spherical coordinates [18]. Our Hamiltonian is still separable in parabolic coordinates (Fig. 1.5):

$$\xi = r + z \tag{1.31a}$$

$$\eta = r - z \tag{1.31b}$$

$$\phi = tan^{-1}(y/x) \tag{1.31c}$$

with operators $\hat{H}$, $\hat{L^2}$, and $\hat{A}_z$, the z-component of the Runge-Lenz vector. Separating our Hamiltonian in parabolic coordinates yields the quantum numbers n, n_1, n_2, and m. These four quantum numbers adhere to the relation

$$n = n_1 + n_2 + |m| + 1 \tag{1.32}$$

and can be re-expressed as n, k, and m when k is written as [2]

$$k = n_1 - n_2 \tag{1.33}$$

The quantum number k is commonly referred to as the electric quantum number [18]. As Hezel et al note [27], A_z can be written as,

$$A_z = \frac{(n_1 - n_2)}{n} = \frac{k}{n} \tag{1.34}$$

The energies to first order of the hydrogen atom in an electric field can then be written as,

$$E = -\frac{1}{2n^2} + \frac{3}{2}nkF \tag{1.35}$$

A very clean derivation of this can be found in Bethe and Salpeter [4]. This energy shift as a function of field strength is the same as found in Eq. (1.27).

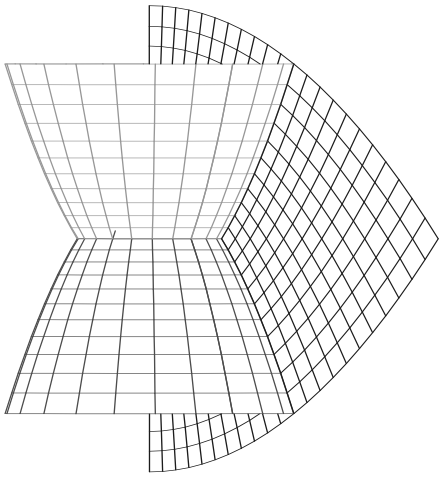

Figure 1.5: Parabolic coordinate system. Lines of constant ξ approach $-\infty$, lines of constant η approach ∞. Rotation through ϕ about the z-axis from 0 to 2π.

From second order time independent perturbation theory, we can calculate the second order energy shift [23],

$$E_n^{(2)} = \sum_{m \neq n} \frac{| < \Psi_m^0 | H' | \Psi_n^0 > |^2}{E_n^0 - E_m^0} \tag{1.36}$$

We can then find the energy to be

$$E_{nkm} = \frac{-1}{2n^2} + \frac{3}{2}nkF - \frac{F^2}{16}n^4[17n^2 - 3k^2 - 9m^2 + 19], \tag{1.37}$$

a downward shift in energy that breaks the m degeneracy of the energy levels [18]. A comparison between the first and second order energy shifts is shown in Fig. 1.6. Perturbation theory can be carried out to greater orders, however the equations quickly become unwieldy. Silverstone has carried these calculations out to 17^{th} order, and notes that anything beyond fourth order is usually unnecessary [49].

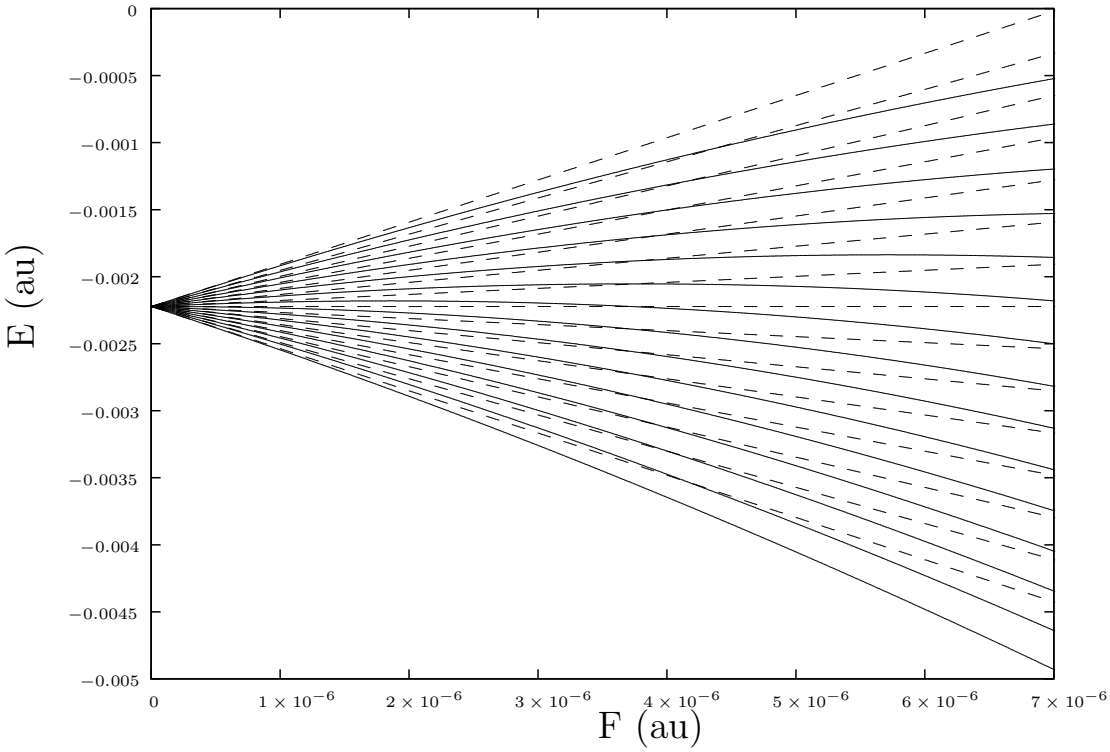

Figure 1.6: Comparison between first and second order Stark shifts for H, $n = 15$, $m = 0$. The dashed lines are the first order shift, the solid lines are the second order shift.

1.2.2 Multi-electron Atoms

While investigating hydrogen provides insight for multi-electron atoms, the change from a single proton to a finite sized core of protons, neutrons, and ground state electrons clearly alters many of our methods of theoretical investigation. The greatest change is that the symmetry of the Coulombic potential is now broken by the ionic core. Our first-order Stark shift now becomes zero as well [18].

For multi-electron atoms, our familiar Rydberg energy equation now becomes,

$$E_n = \frac{-1}{2(n - \delta_l)^2} \tag{1.38}$$

where δ_l is an empirically determined, l dependent number known as the quantum defect. This quantum defect also represents a phase shift in the quantum wave-function of the atom [26, 36].

Due to the finite sized core of the atom, n_1 is no longer a good quantum number and therefore our atom is not separable in parabolic coordinates. The greatest implication of n_1 no longer being a good quantum number is a coupling between the red (down-shifted) and blue (up-shifted) states of the atom [18]. As a result, avoided crossings exist in the energy spectra of non-hydrogenic atoms [50]. These avoided crossings alter the classical dynamics of Rydberg atoms and provide the deviations from the simple hydrogenic dynamics derived above. A powerful technique for understanding the dynamics of highly excited multi-electron atoms is closed orbit theory, which will be discussed in Sec. 2.4.

1.3 Previous Research

Previous research in the Morgan Lab has focused on Rydberg helium [32, 34–36] and Rydberg argon [16, 33]. Much work by other groups has been conducted on the alkali metals, both experimentally and theoretically [47, 57]. Our lab next looks to investigate excited xenon in an electric field. Research into Rydberg xenon seems to have first been undertaken by Stebbings et al in 1975 [51, 56]. However, this work was done only for the zero-field case. Other previous work on xenon has primarily been done by Knight and Wang [37, 38, 54] and Ernst et al [15]. Knight and Wang's research is primarily at zero-field [37, 54], with one investigation of xenon in an electric field for a small energy range around $n = 17$ [38]. Ernst et al have only investigated the n range between 14 and 21.

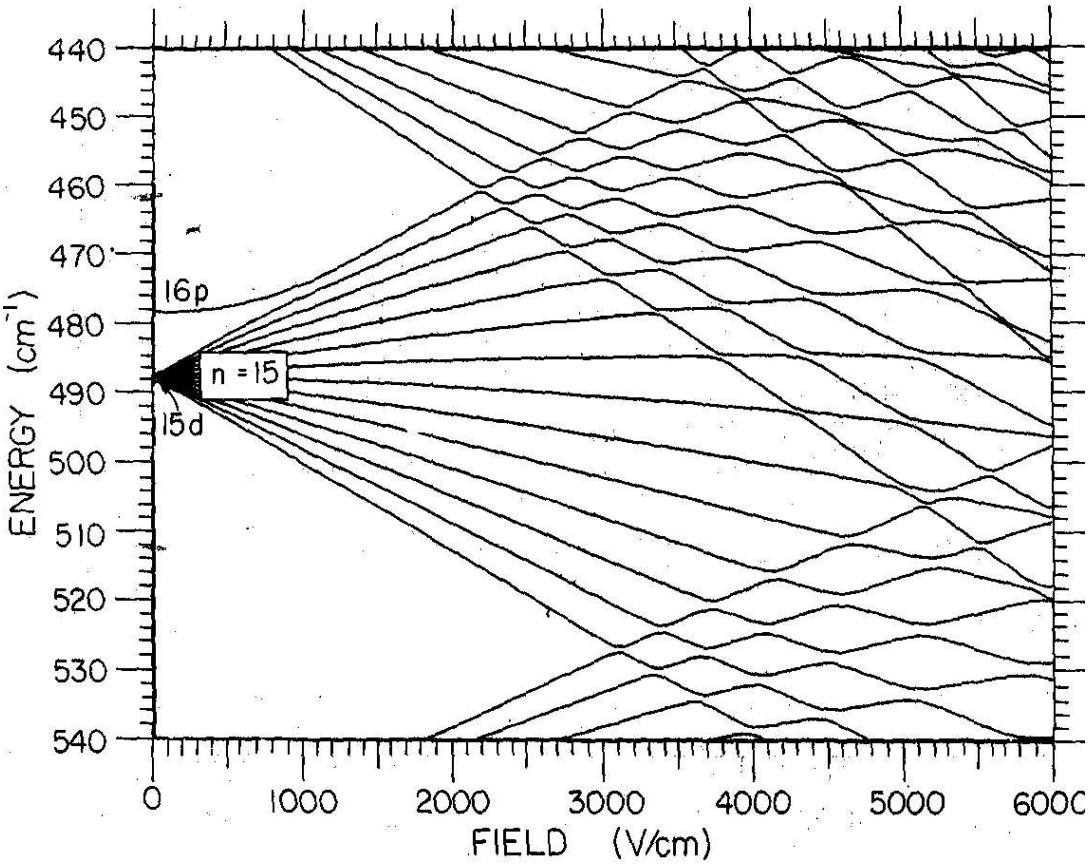

Figure 1.7: Example of avoided crossings. Stark Rydberg sodium absorption calculation from [57].

Warntjes et al have previously investigated the decay paths of autoionizing Rydberg xenon Stark states [55]. Optogalvanic spectroscopy has also been done on Rydberg xenon for the zero-field case [39]. In the next chapter we will introduce a powerful method of spectral investigation known as recurrence spectroscopy. No previously published recurrence spectra have been taken for xenon.

Chapter 2

Methodologies of Spectroscopy

2.1 Absorption Spectra

Recurrence spectroscopy begins with first taking absorption spectra. An atom absorbs energy at specific quantized energy levels, and absorption spectra such as Fig. 2.1 represents a plot of the available energy levels for helium over the energy range from $n = 19$ to $n = 30$.

As we add an external electric field to our system in our experiment, the total system energy changes accordingly,

$$H = \frac{p^2}{2} - \frac{1}{r} + Fz \tag{2.1}$$

However, we can scale our Hamiltonian variables r and p so that our Hamiltonian is invariant in an electric field. As Keeler describes [32], we can find the scaling

variables,

$$r = F^{-1/2}\tilde{r} \tag{2.2a}$$

$$p = F^{1/4}\tilde{p} \tag{2.2b}$$

$$z = F^{-1/2}\tilde{z}. \tag{2.2c}$$

We can fold these ideas into a scaled energy relation, which we will refer to as epsilon. Our scaled energy is then defined as

$$\epsilon = E/\sqrt{F} \tag{2.3}$$

A full derivation can be found in Appendix B. For a given ϵ our system Hamiltonian is now completely independent of the external electric field applied to it. We therefore scale our absorption spectroscopy accordingly, altering our electric field and laser energy to keep ϵ constant. This holds the classical dynamics of the system constant.

Our spectroscopy is conducted using the second harmonic of a pulsed 1064nm Nd:YAG (Neodymium doped Yttrium Aluminum Garnet) laser pumping a home-made dye laser. The light from the dye laser is then sent through a doubling crystal. This method gives us a laser bandwidth of less than 0.5 cm^{-1} with a wide tunable range over multiple tens of wavenumbers [32]. Selection of the magnetic angular momentum state (quantum number m) investigated is dependent on the polarization of the laser with respect to the electric field. Laser polarization parallel to the applied electric field corresponds to $m = 0$ and polarization perpendicular to the field yields $m = 1$ excitation [16].

Successive scans are taken with the laser for different ϵ values. These scans are then collated together to form a scaled absorption map.

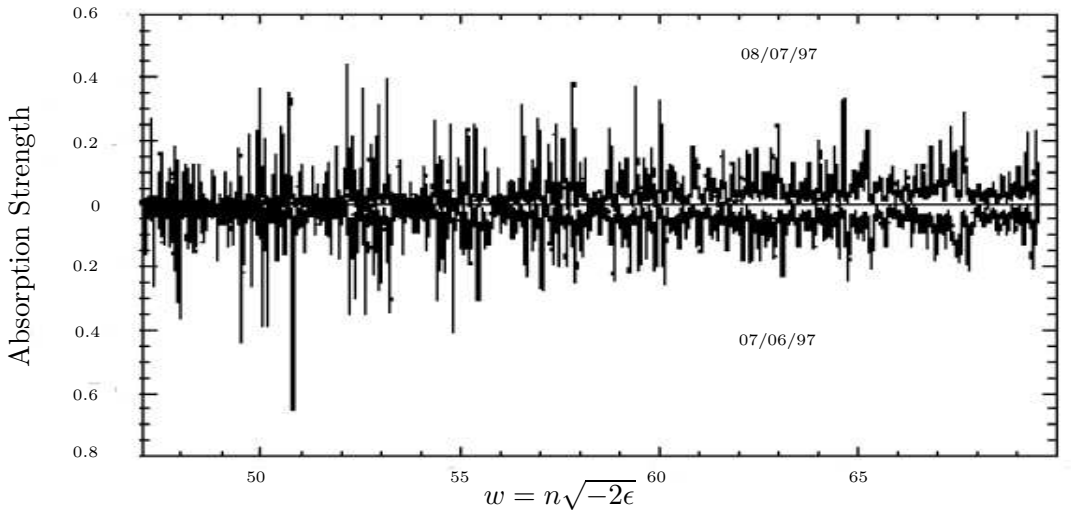

Figure 2.1: Absorption spectra of $\epsilon = -2.7$, $m = 0$, triplet state of helium, taken by Len Keeler in the Morgan Lab on July 6th, 1997 and August 8th, 1997 [32].

2.2 Fourier Transforms

Any mathematical function, $f(x)$, can be broken down into a superposition of sine and cosine functions. This notion is known as Fourier analysis [17]. This idea can be mathematically represented as

$$f(x) = \sum_{n=-\infty}^{\infty} C_n e^{ikx} \tag{2.4}$$

where $k = n\pi/a$ for a function in the domain $[-a, a]$.

The function $\mathscr{F}(f(x))$ or $F(k)$ that represents the C_n components of $f(x)$ is referred to as the Fourier transform of $f(x)$.

$$F(k) = \int_{-\infty}^{\infty} f(x) e^{-ikx} dx \tag{2.5}$$

where k is known as the conjugate variable of x [3]. In essence, the Fourier transform represents what periodic structures exist in a function.

For an example, we can look at the function

$$f(x) = \cos(x) + 2\cos(3x) + \cos(7x) \tag{2.6}$$

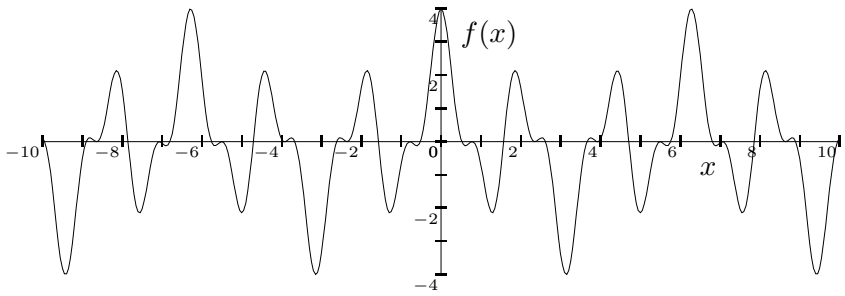

Figure 2.2: A plot of Eq. (2.6)

A plot of this figure is shown in Fig. 2.2. The Fourier transform of this function can be written as

$$F(k) = \pi(\delta(k-1) + \delta(k+1) + 2\delta(k-3) + \delta(k+3) + \delta(k-7) + \delta(k+7)) \tag{2.7}$$

where $\delta(x)$ is a Dirac delta function: infinity at x, zero elsewhere, and has an area of one. A representation of this transform is shown in Fig. 2.3.

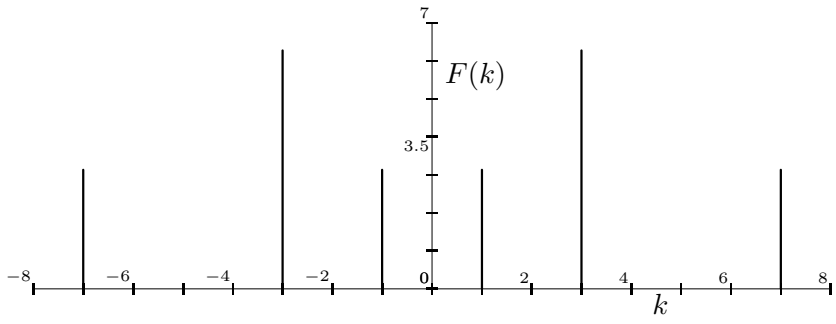

Figure 2.3: Fourier transform of Eq. (2.6).

2.3 Recurrence Spectra

We take the Fourier transform of the scaled absorption spectra to create recurrence spectra. Recurrence spectra is the square of the Fourier transform of absorption spectra. In practice, this Fourier transform is usually done using a method known as a Fast Fourier Transform, or FFT [31]. The Fourier transform of the above absorption spectra (Fig. 2.1) is shown in Fig. 2.4. The Fourier transform of our scaled absorption spectra leads to a plot in the domain of scaled action ($\tilde{S}$).

Classically, the principle of least action defines the correct motion of a particle. Action is defined as,

$$\tilde{S} = \oint \tilde{p} \cdot \mathrm{d}\tilde{q} \tag{2.8}$$

where $\tilde{q}$ and $\tilde{p}$ are the scaled generalized position and momentum variables [32]. Given a particle's action and energy, one can calculate the entire classical trajectory of a particle from it's initial launching angle [22].

2.4 Closed Orbit Theory

Closed orbit theory is one of the most powerful techniques for interpreting atomic recurrence spectra. Closed orbit theory uses semi-classical methods for the path of the electron far away from the nucleus, and quantum mechanical wavefunctions close to the nucleus. For this idea to work, the classical trajectories must include the same phase information as the quantum mechanical wavefunctions [32]. The crux of closed orbit theory is that there exists a "complementary principle", where each quantum mechanical energy level can be associated with a family of trajectories and periodicities in the quantum mechanical spectrum can be asso-

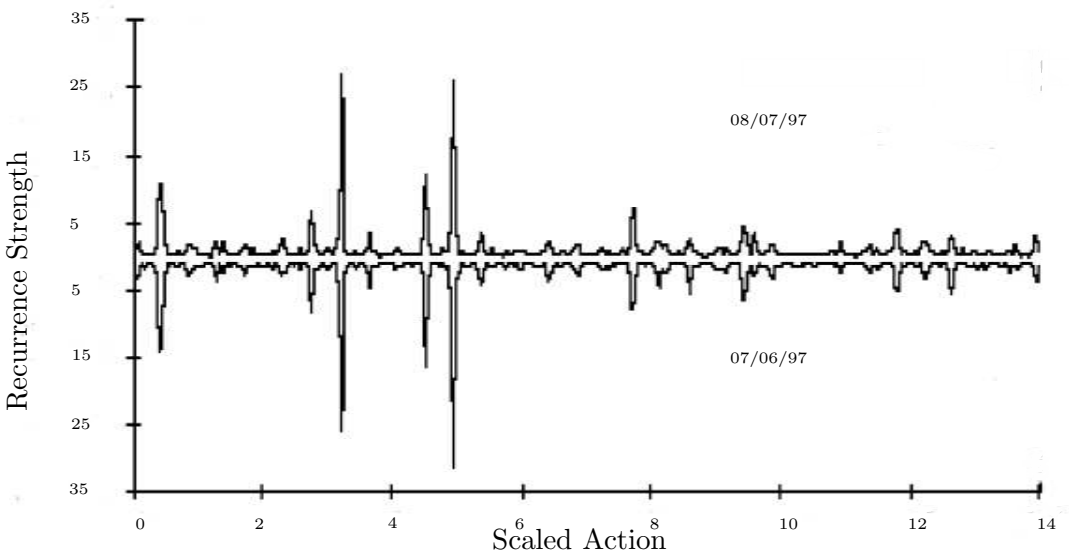

Figure 2.4: Recurrence spectra of Fig. 2.1 taken by Len Keeler in the Morgan Lab [32]

ciated with a single closed orbit [30]. Initially, the excited electron is formulated to be an outgoing wavefront. Away from the nucleus this wavefront is considered as a set of trajectories. These trajectories form an incoming wavefront that interferes with the outgoing wavefront to create oscillations in the absorption spectra [14].

Closed orbit theory originated primarily from work by Delos, Du, and Gao [12–14, 19–21, 24, 48]. Closed orbit theory has grown into a strong bridge over the gap between semi-classical and quantum mechanical physics in these highly excited systems. Taking the Fourier transform of our absorption spectra lets us assign specific trajectories to lines in the absorption spectra. The Fourier transform illustrates the periodicities in the quantum mechanical structure. These trajectories can be labeled as ratios of rational numbers, u/v, corresponding to

a ratio of angular frequencies of the orbit in parabolic coordinates [16]. This gives us the ability to relate classical orbital dynamics to the quantum mechanical spectra taken by our apparatus. A more thorough investigation of closed orbit theory can be found in the doctoral theses of Len Keeler and Heric Flores-Rueda [16, 32].

Chapter 3

The Portable Rydberg Generator

3.1 Overview of Design

Previous experimentation in the Morgan Lab employed the use of collinear fast-atom beam technology for conducting laser spectroscopy. Maintaining a 10 keV particle accelerator for conducting research brings along large and often unnecessary headaches. As well, due to the limitations of some of the materials of the ion source, a finite operating uptime is usually limited to less than one hundred hours [32].

A new very small apparatus was designed by Len Keeler to fit in an MDC Del-Seal flange $3 - 3/8''$ six-way cross vacuum chamber. Combined with a diffusion pump, mechanical pump, and small rack of power supplies, this new apparatus was designed with the idea that the apparatus could be moved to any available laser, with laser time being a precious commodity. Because of this notable quality, the new apparatus was dubbed "The Portable Rydberg Generator", or PRG for short (see Fig 3.1 for a schematic diagram and Appendix E for pictures).

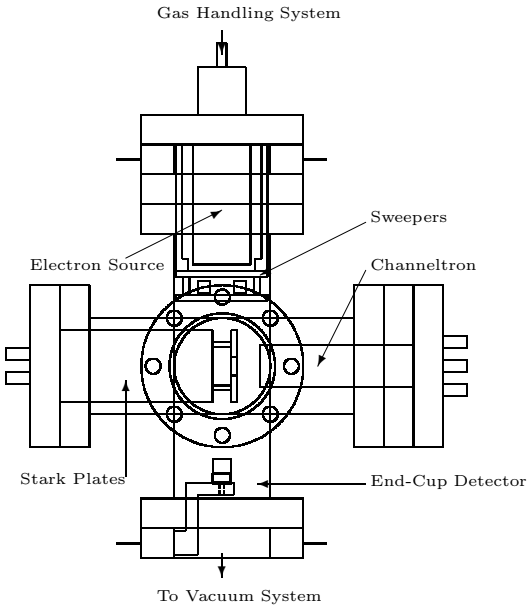

Figure 3.1: Diagram of PRG

Whereas the previous apparatus (still impressively maintained and used by David Wright) utilizes fast beam charge transfer as its means of creating metastable atoms [30], the PRG uses electron impact. Electrons transversely collide with a diffusive gas jet of ground state atoms for excitation to the metastable state. The metastable beam is then sent past a positively charged plate. This plate sweeps away any stray charged particles while the neutral metastable atoms are unaffected (Fig. 3.4 and Fig. 3.5). The metastable beam then simultaneously passes through the laser interaction region and Stark field. Finally, the Stark field is then pulsed higher to ionize the created Rydberg atoms. These ions are then detected by the use of a Channeltron ion detector. Metastable production is measured by way of a nickel Faraday cup (Fig. 3.2 and Fig. 3.3) whose work function is lower than the metastable potential energy.

One of the great benefits of the PRG is its insensitivity to a specific gas. The

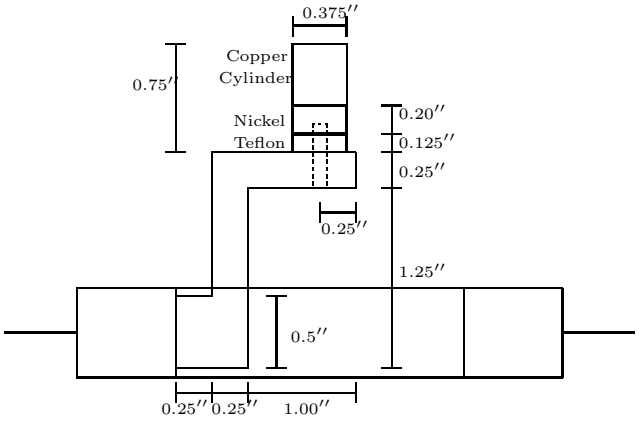

Figure 3.2: End-cup assembly (Side View)

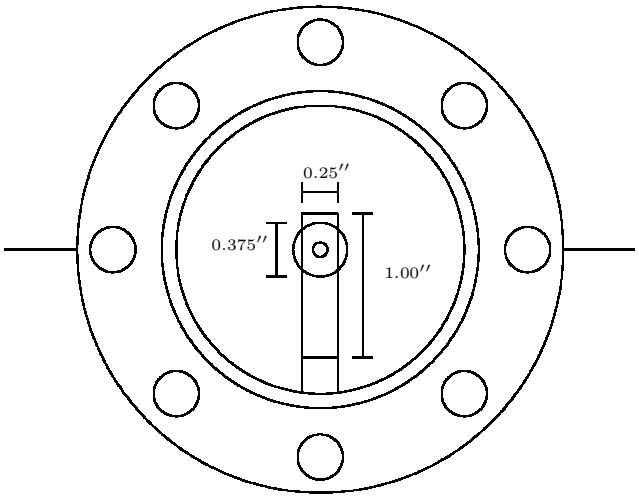

Figure 3.3: End-cup assembly (Top View)

only species dependent aspect of the metastable creation stems from the momentum transfer of the electron collision. Lighter thermal gas beams are deflected more by the electron collision than heavier species. Although the Colutron ion source of the other apparatus takes a wide range of species, the gas used in the cell for the charge transfer is dependent on the gas being excited [16]. Altering the PRG for a different gas species requires only flushing the gas tube, changing the gas bottle, and adjusting the electron source energy.

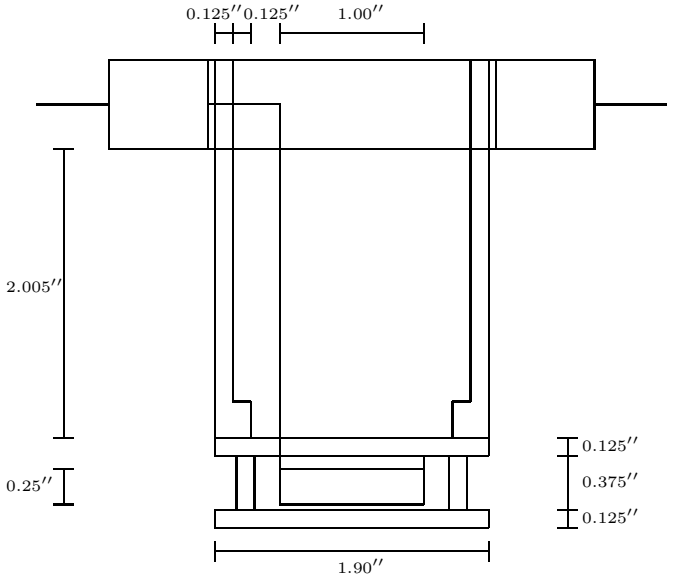

Figure 3.4: Diagram of charged particle sweepers (Side View)

3.2 Metastable States

3.2.1 Metastable Hydrogen

Excitation from the ground state to a high lying Rydberg state, such as n=15, requires more than 99.5% of the energy needed to ionize an electron from a

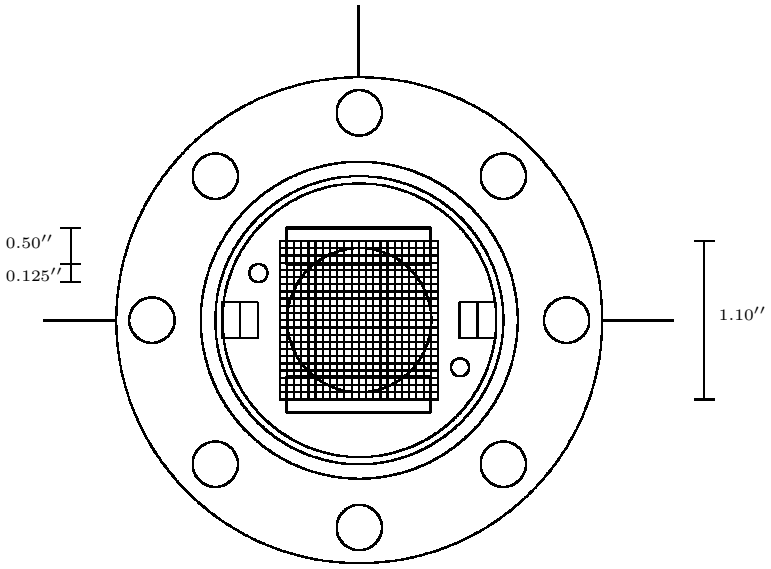

Figure 3.5: Diagram of charged particle sweepers (Top View)

hydrogen atom. Even laser excitation in the H atom from the ground state to the first excited state requires a photon of 121.5 nm, by the Rydberg equation

$$\frac{1}{\lambda} = R(\frac{1}{n_f} - \frac{1}{n_i}) \tag{3.1}$$

where R is the Rydberg constant, equal to 1.097×10^7 m^{-1}. Exciting to the n=15 state requires a 91.5 nm photon, well out of the visible spectrum and into the UV. Tunable, coherent, monochromatic ultraviolet laser sources are usually expensive and/or difficult to construct [15], and therefore experimentalists have sought other means for bridging the energy gap between the ground state of many atoms and their energetic Rydberg states [18, 38].

If we look at the dipole selection rules that govern the transitions between

states of a hydrogen atom,

$$\Delta m = \pm 1, 0 \tag{3.2a}$$

$$\Delta l = \pm 1 \tag{3.2b}$$

we can generate a diagram of the decay paths of the first four levels of H (see Fig 3.6). There is no decay route for the hydrogen $2s$ level to decay to the ground state via spontaneous emission. This state is known as the metastable state and is long-lived ($\sim$0.2 seconds for H [23,41]). Excitation from the hydrogen metastable state to the n=15 state requires a 371.2 nm photon, obtainable by a dye laser and doubling crystal. Excitation to the metastable state is done by a variety of means [15, 18, 32], most notably charge exchange and electron impact.

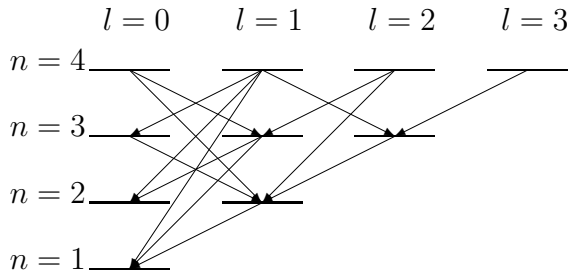

Figure 3.6: Decay routes by spontaneous emission of the first four energy levels of hydrogen governed by dipole selection rules.

3.2.2 Multi-Electron Metastable States

As Bethe and Salpeter describe [4], selection rules can be abstracted to any general atom as

$$\Delta m = 0, \pm 1 \tag{3.3a}$$

$$\Delta J = 0, \pm 1 \tag{3.3b}$$

$$J = 0 \not\rightarrow J = 0 \tag{3.3c}$$

where J is the sum of the total system orbital and spin angular momenta. If the spin-orbit coupling is small (notably for low atomic number) and L and S are reasonably good quantum numbers, the Russell-Saunders approximation is valid [10]. In this case, four other selection rules also apply:

$$\Delta\Psi_{\text{parity}} : \quad g \rightarrow u, \quad u \rightarrow g \tag{3.4a}$$

$$\Delta L = 0, \pm 1 \tag{3.4b}$$

$$L = 0 \not\rightarrow L = 0 \tag{3.4c}$$

$$\Delta S = 0 \tag{3.4d}$$

Argon has two important metastable states[1], $3p^5 4s\ ^3P_2$ state and $3p^5 4s\ ^3P_0$ state [5]. Xenon likewise has two notable metastable states, the $5p^5 6s\ ^3P_2$ state and the $5p^5 6s\ ^3P_0$ state [37].

3.2.3 Methods of Metastable Creation

Charge Transfer

One of the more experimentally popular methods for creating metastable atoms is a method known as charge transfer or electron capture [46]. A beam of accel-

[1] Denoted $^{2S+1}L_J$.

erated ions is sent through a thermal vapor or gas and the ions capture valence electrons from the vapor (or gas) [11]. Experimental research by Il'in pointed to much higher efficiencies of electron capture of fast-atoms beams with alkali metal vapors than gases, by up to a factor of five [28, 46]. This experimental work also confirmed the theoretical research of Oppenheimer [44] and Jackson [29] that charge transfer from thermal atoms to fast ions populates n-states as $1/n^3$.

The choice of gas or alkali metal vapor is primarily dependent on two factors, one practical, one physical. First, the species is experimentally easy to work with; the substance has a relatively low vaporization temperature, is non-toxic, is non-reactive, etc. The other criteria is a small energy defect between the species and the atomic beam excited metastable state [11]. The Morgan Lab has primarily used sodium and potassium metals for charge transfer [11, 16, 32, 33, 46].

In practice, neutralization rates between forty and fifty percent occur [32]. The neutralization rate can be adjusted by the temperature of the vapor. However, increasing the vapor temperature increases the number of multiple collision events. Multiple collisions can directly de-excite a metastable, further excite a newly created metastable atom to ionization or to a further excited state (quickly decaying back to the ground state). Using sodium for metastable helium creation, Len Keeler found up to 75% of created neutrals were in the 2^3S metastable state.

Electron Impact

Electron impact has not previously been used for recurrence spectroscopy in the Morgan Lab. Electron impact is simply colliding a gas with energetic electrons corresponding to the energy gap of the desired excitation [1]. Therefore, creation

of metastable states from a ground state gas requires accelerating electrons to the energy of the metastable state. The electron collides with a gas particle and the energy transfer excites the ground state electron to the metastable state.

The drawback of this technique is the momentum transfer from the accelerated electron inelastically colliding with the gas particle. This effect is small or even negligible for heavy atoms (such as Ar or Xe) but will heavily deflect a thermal beam of light atoms [42]. Tommasi et al report a 12° deflection for helium-electron collisions to the 2^3S_1 and 2^1S_0 metastable states [52].

3.3 Electron Sources

3.3.1 HeatWave Labs Source

The original electron source for our apparatus was purchased from HeatWave Labs, Inc. in Watsonville, California. We purchased a STD 400 TB-198 Standard Series Barium Tungsten Dispenser Cathode from HeatWave Labs. This source is reported by the manufacturer to yield $2.5 - 4.0$ A of electrons with an operating lifetime greater than ten thousand hours. [25]

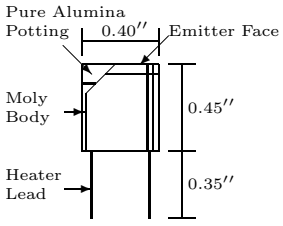

Figure 3.7: Diagram of HeatWave TB-198 standard series barium tungsten dispenser cathode

However, we were unable to obtain lifetimes greater than roughly one hun-

dred hours without cathode surface pitting and only marginal electron output. We also had difficulty fitting these sources into our apparatus without overly stressing the leads to the source. The high operating temperatures of these sources, above one thousand degrees Celsius, made it difficult to use any materials in our apparatus other than stainless steel (which out-gasses impurities at such high temperatures) and ceramic[2]. Due to the cost of these electron sources ($562/source) and the difficulty in operating them, we soon looked for other electron sources.

3.3.2 Southwest Vacuum Devices Source

On the further recommendation from Len Keeler, our lab contacted Southwest Vacuum Devices. They sell electron guns and emission products, primarily for televisions and industry. However, their C–14 cathode and related H–61 heaters suited our needs quite well. Together the cathodes and heaters sell for around thirteen dollars. Very little concrete documentation on these products was available from Southwest Vacuum Devices. The cathode is rated to produce around 600 mA off a surface roughly an eighth of an inch in diameter. Unlike the previous HeatWave Labs electron source, two of these electron sources can be run in parallel in the PRG.

3.4 Operating Parameters

The first part of getting the PRG operational was investigating whether or not we can generate metastable atoms. We started with argon gas rather than xenon

[2]Experimenters take note: Aluminum melts at 660.37°C [8]

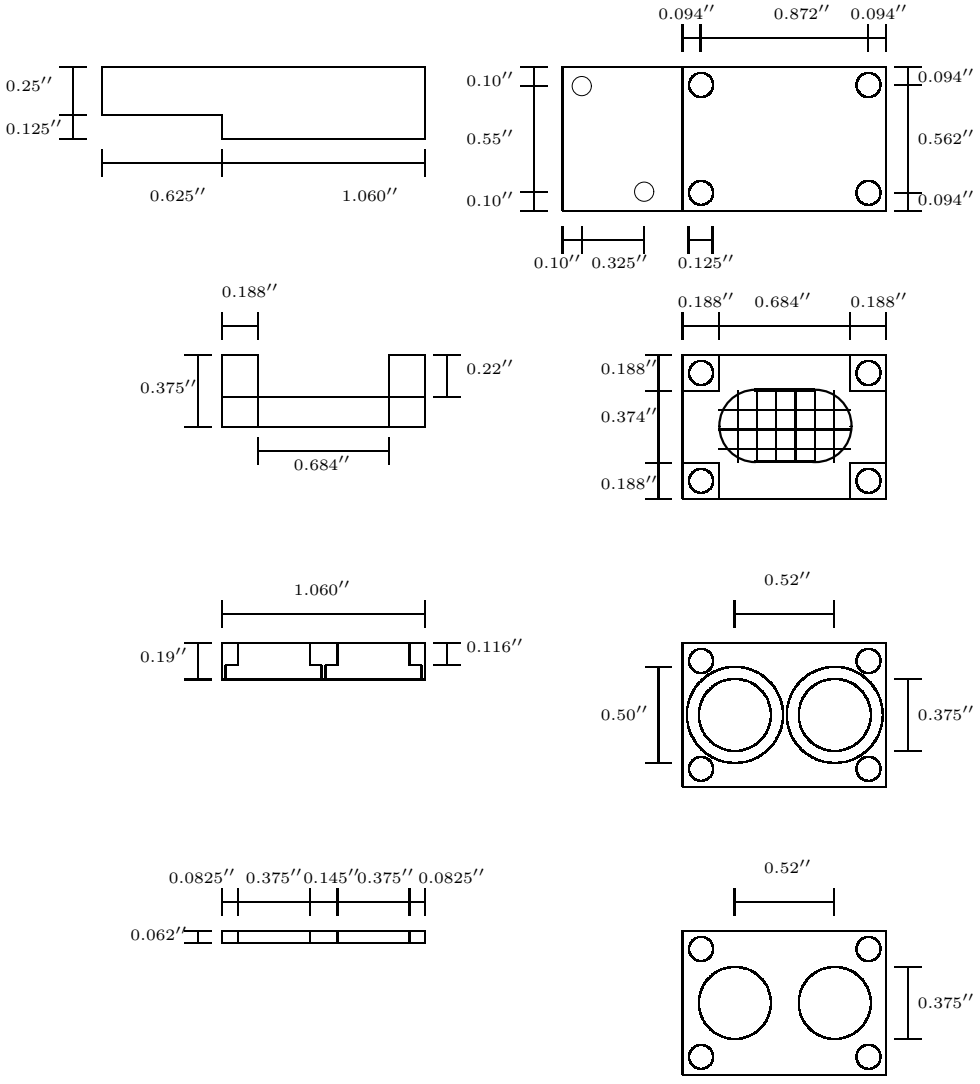

Figure 3.8: PRG electron source (Side and Exploded Top View) (SW-Vacuum Device Configuration)

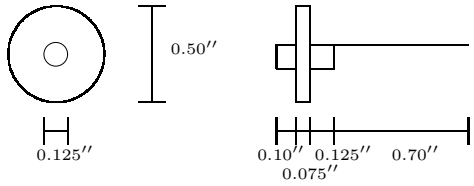

Figure 3.9: Southwest Vacuum Devices $C-14$ cathode diagram

for our initial experiments. Recent experimental argon data by David Wright on the other apparatus in the Morgan Lab gave us experimental data to check our results to. Xenon is also more expensive compared to argon. We first biased our nickel end-cup by 27 V using three 9 V batteries. After warming up our electron sources and letting them stabilize, we measured the current from the end-cup as we increased the electron energy from eight to twenty-four electron-volts. Nickel has a low electron work function of 5.15 eV [8]. Colliding the nickel with energetic neutral thermal atoms generates a current in the nickel from secondary electron emission that can be measured with a picoammeter.

We first measured the background signal by measuring the end-cup current with no argon gas in the system, a background pressure around 2×10^{-7} torr, and the sweepers off for electron accelerations between eight and twenty-four volts. This negative background signal therefore stems from stray electrons from the electron source and other errant charged particles in the apparatus. Next, a potential of approximately one hundred and forty volts was placed on the sweepers to keep stray electrons from reaching the end-cup and the end-cup current was once again measured for electron acceleration voltages of eight to twenty-four volts. Argon gas was next introduced into the system to a total pressure of 4.2×10^{-6} torr. The current from the end-cup was once again measured for electron acceleration voltages between eight and twenty-four volts with the sweepers

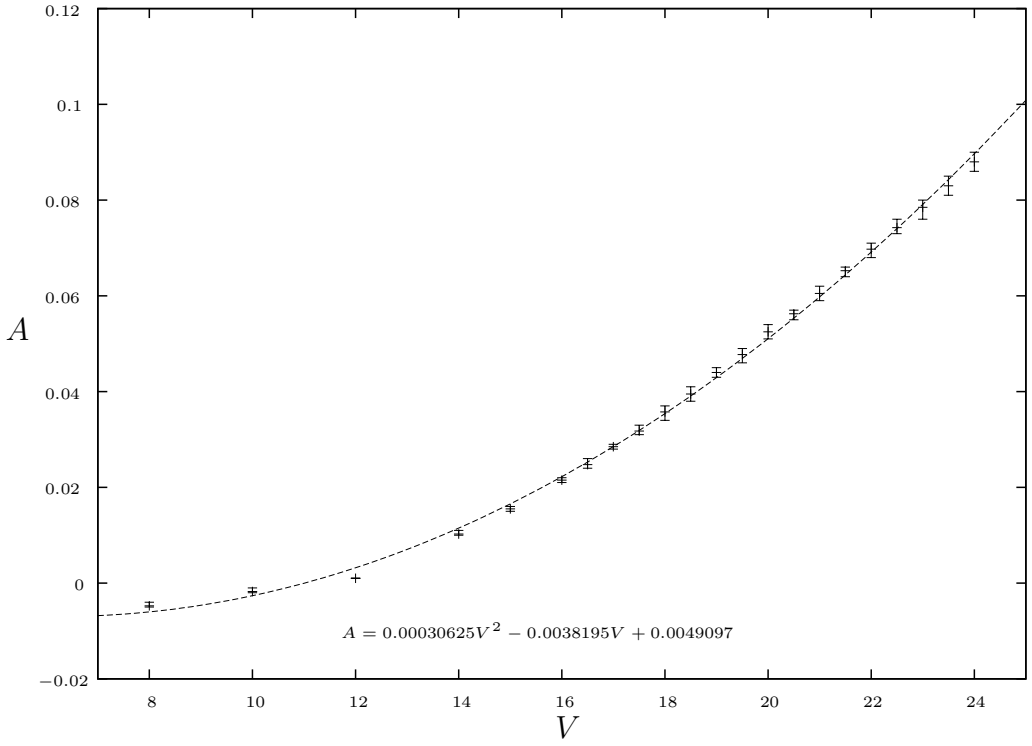

Figure 3.10: Electron source output current (A) of Southwest Vacuum Devices source as a function of acceleration voltage (V). Electron Source heaters were at 12 V, drawing $\sim$2 A.

off and then on. Argon has a metastable energy of 11.55 eV [43] and an ionization energy of 15.76 eV [53]. Therefore, we should start to see metastable atoms being made just at 11.55 eV, with the metastable production increasing until ionization takes over past 15.76 eV. This data was then analyzed to see if metastable argon atoms were being produced.

Chapter 4

Experimental Data and Analysis

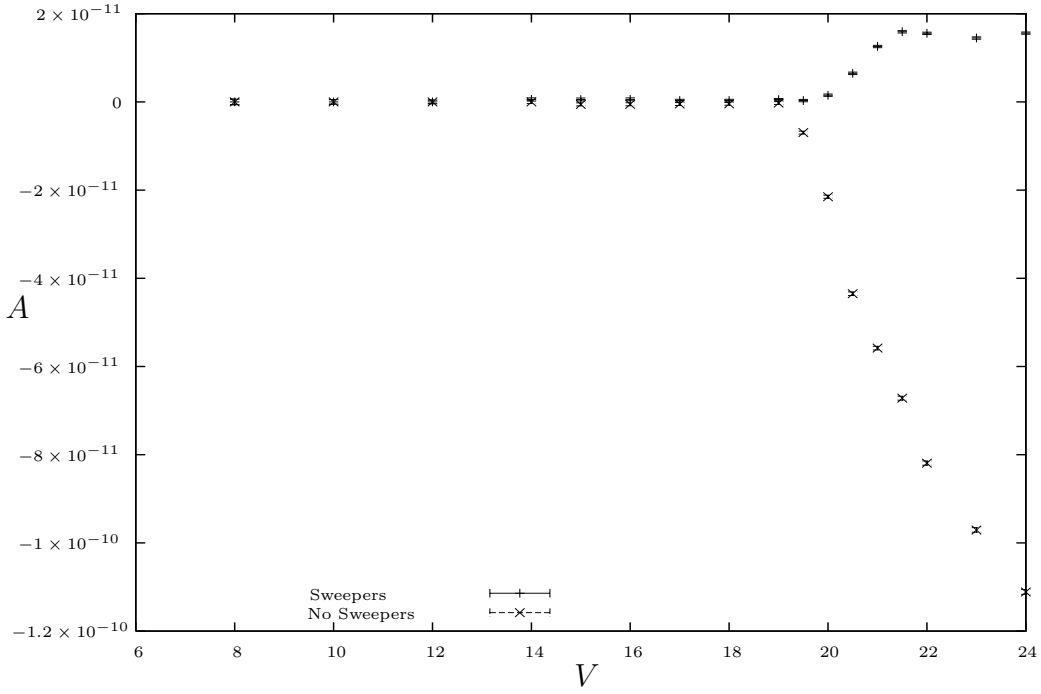

Figure 4.1: Experimental argon data illustrating production of metastables by HeatWave source. Plot of normalized end cup current (arb. units) as a function of electron acceleration voltage(volts)(07/09/03).

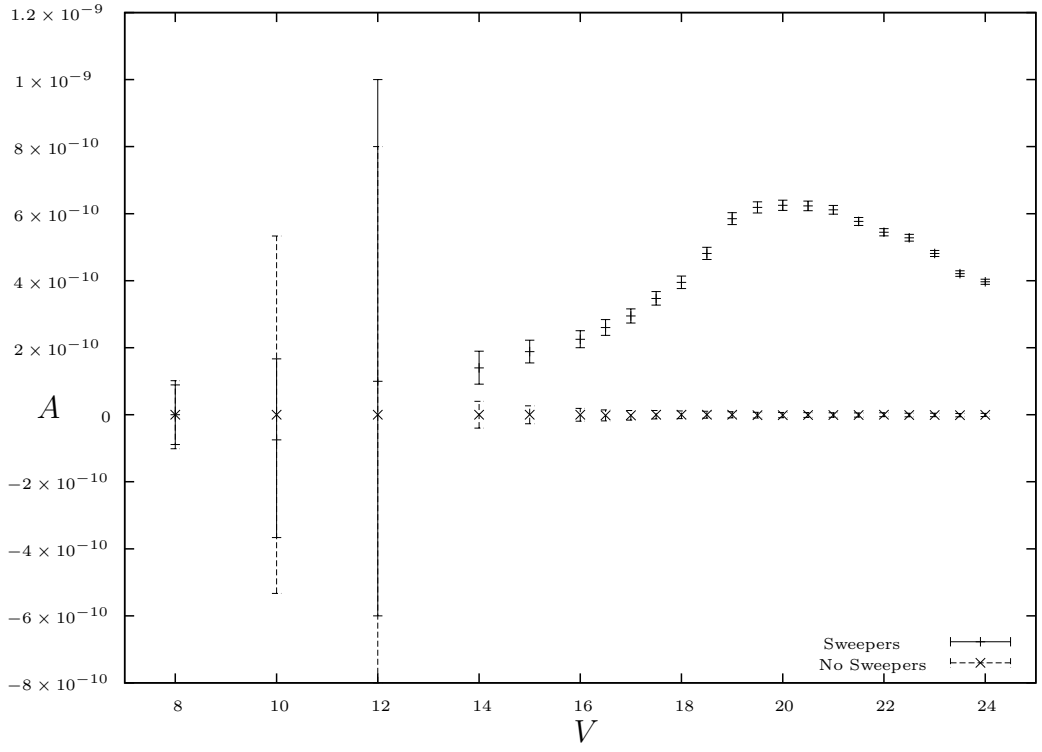

Figure 4.2: Experimental argon data illustrating production of metastables by Southwest Vacuum Devices source. Plot of normalized end cup current (arb. units) as a function of electron acceleration voltage(volts)(1/23/04).

The feasibility of the new PRG apparatus hinged on its ability to create metastable states. A large effort was made to ensure that the machine was actually creating metastable argon atoms by electron impact.

To analyze the experimental metastable data, the initial background end-cup current was first subtracted from all the data. This data was then normalized by dividing the end-cup current by the electron source current. Finally, our end-cup current when no gas is in the system is subtracted away from the end-cup current when gas is fed into the system.

$$\text{Signal} = \frac{\text{end-cup}_{\text{gas}} - \text{background}_{\text{gas}}}{\text{source}_{\text{gas}}} - \frac{\text{end-cup}_{\text{no gas}} - \text{background}_{\text{no gas}}}{\text{source}_{\text{no gas}}} \quad (4.1)$$

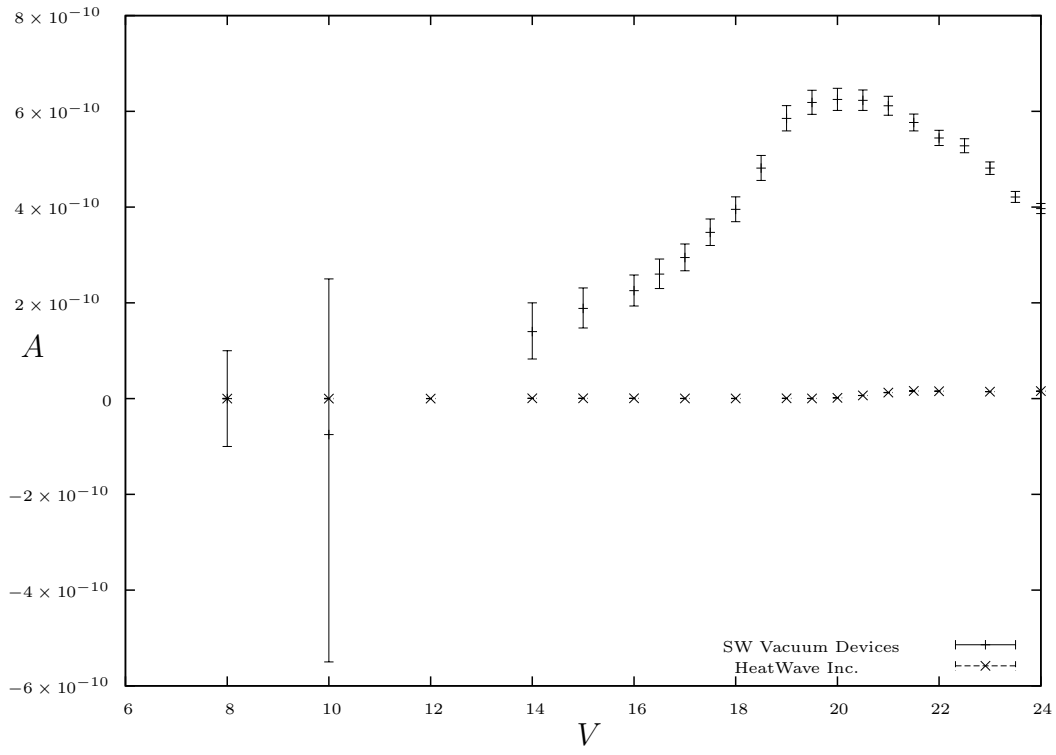

Figure 4.3: Comparison of experimental argon metastable data from Fig. 4.1 and Fig. 4.2.

Plots of the normalized signal vs electron acceleration voltage can be seen in Fig. 4.1 (HeatWave source) and Fig. 4.2 (Southwest Vacuum Devices source). The points in these plots are of experimentally measured data, while the error bars in these plots are the range given by the precision of our measurement devices. This signal represents excitation to both the $^3P_0$ and $^3P_2$ metastable states of argon.

Although the Southwest Vacuum Devices sources produces a much smaller electron current than the HeatWave electron sources, the Southwest Vacuum Devices source is much more efficient in its metastable production. The normalized, sweepers on, end-cup current from the two sources is compared in Fig. 4.3.

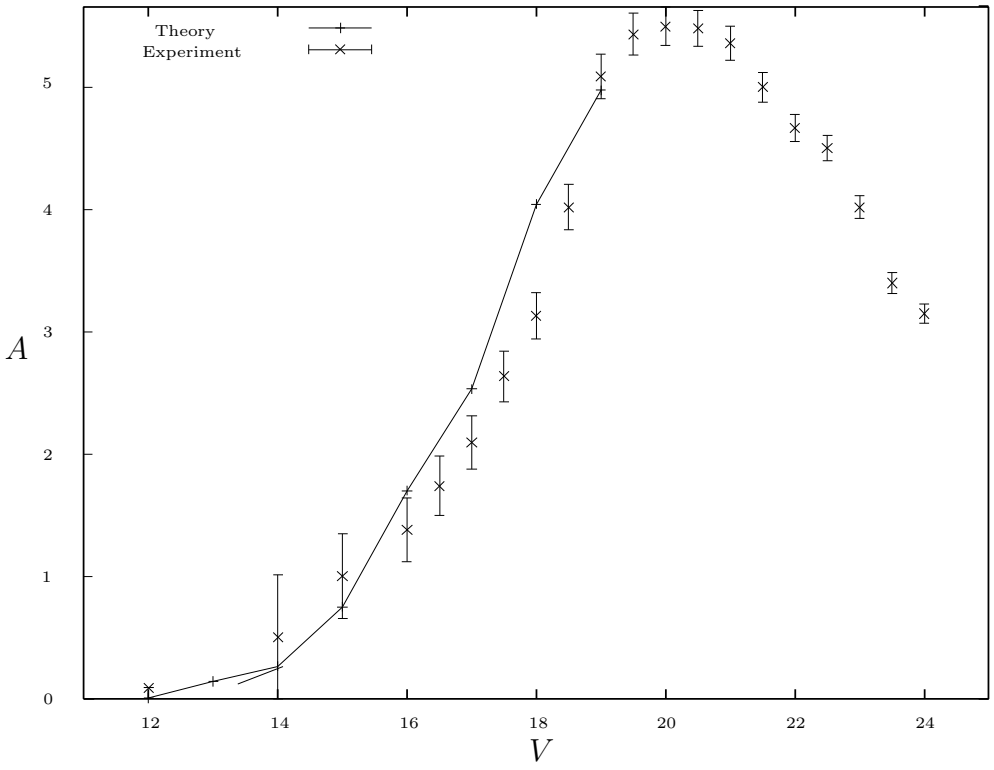

Figure 4.4: Comparison of experimental argon data and known apparent electron impact excitation cross sections (arb. units) as a function of electron energy (volts). Cross section data taken from [6, 45].

This efficiency is not terribly surprising, as that the surface area of the HeatWave source is much larger than the atomic beam path area. Therefore, most of the electrons from the HeatWave electron gun never interact with a gas atom.

On comparison of our experiment data with other experimental data [6] and theoretical analysis [7, 45], as shown in Fig. 4.4, we can conclude that argon metastable atoms are successfully being created by our apparatus.

Chapter 5

Conclusion and Future Work

Our lab has not yet successfully taken absorption spectra with our new apparatus. However, we have certainly seen the feasibility of using electron impact as a method for creating metastable atoms.

Difficulties in obtaining absorption spectra from the new apparatus come from an overwhelming background absorption signal on our Channeltron detector. The laser beam seems to not only excite our desired beam of atoms, but background gas as well, even at Ultra-High Vacuum pressures. In our previous experiments we have been able to steer our fast-atom beam towards our ion detector with electric fields [32]. This method has let us separate our excited beam from our excited background noise. However, our thermal beam passes directly in front of our Channeltron detector and cannot be easily separated from the background signal. We continue to search for a clean absorption signal from the Portable Rydberg Generator.

As stated earlier, our eventual goal is to take scaled recurrence spectra of Rydberg xenon in Stark fields. An interesting area of investigation may be

utilizing the electron impact source with the particle accelerator used in previous experiments in the Morgan Lab. After investigating xenon, our lab looks to begin research into scaled recurrence spectroscopy of Rydberg molecular hydrogen. As Professor Tom Morgan likes to tell his lab group, "The future is molecules!"

Appendix A

Stark Frequency Derivation

This derivation comes from Hezel et al [27], but is included for completeness. We can first begin with Hamilton's equations:

$$\dot{\vec{p}} = -\vec{\nabla}_r H \tag{A.1a}$$

$$\dot{\vec{r}} = \vec{\nabla}_p H \tag{A.1b}$$

for the Hamiltonian,

$$H = H_{\text{Coulomb}} + V(\vec{r}) \tag{A.2}$$

From this we can generate the change in momentum as

$$\dot{\vec{p}} = \dot{\vec{p_c}} - \vec{\nabla} V(\vec{r}) \tag{A.3}$$

By manipulating the definition of angular momentum,

$$\vec{L} = \vec{r} \times \vec{p}, \tag{A.4}$$

to find the change in angular momentum,

$$\dot{\vec{L}} = \dot{\vec{r}} \times \vec{p} + \vec{r} \times \dot{\vec{p}} \tag{A.5}$$

Substituting our Hamiltonian into Eq. (A.5) and noting that

$$\dot{\vec{L}_c} = 0 \tag{A.6}$$

we find

$$\dot{\vec{L}} = -\vec{r} \times \vec{\nabla} V(\vec{r}) \tag{A.7}$$

The gradient of potential is the electric field, $\vec{F}$. Eq. (A.7) can therefore be rewritten as

$$\dot{\vec{L}} = -\vec{r} \times \vec{F} \tag{A.8}$$

The change in angular momentum is torque, written as,

$$\dot{\vec{L}} = \vec{\tau} \tag{A.9}$$

Due to the rapid motion of the electron,

$$< r >= - < d > \tag{A.10}$$

Note that by applying Eq. (A.9) and Eq. (A.10) to Eq. (A.8) yields the expression for the torque of a dipole,

$$\vec{\tau} = \vec{d} \times \vec{F} \tag{A.11}$$

From Eq. (1.25), the average distance can be written as

$$< d >= \frac{3}{2} n^2 \vec{A} = - < r > \tag{A.12}$$

This makes our change in angular momentum

$$\dot{\vec{L}} = \frac{3}{2} n^2 (\vec{A} \times \vec{F}) \tag{A.13}$$

Setting $\vec{F} = F_z$ makes $\dot{L}_z = 0$. L_z is therefore a conserved quantity and usable as a commuting operator for the Stark effect in parabolic coordinates.

We can derive a similar expression for $\dot{\vec{A}}$ in the following manner. Taking the derivative of the definition of $\vec{A}$ leads to

$$\dot{\vec{A}} = \dot{\vec{p}} \times \vec{L} + \vec{p} \times \dot{\vec{L}} - \dot{\hat{r}} \tag{A.14}$$

We can substitute Eq. (A.3) for $\dot{\vec{p}}$,

$$\dot{\vec{A}} = (\dot{\vec{p_c}} - \vec{\nabla} V(\vec{r})) \times \vec{L} + \vec{p} \times \dot{\vec{L}} - \dot{\hat{r}} \tag{A.15}$$

$$\dot{\vec{A}} = (\dot{\vec{p_c}} \times \vec{L} - \dot{\hat{r}}) - \vec{F} \times \vec{L} + \vec{p} \times \dot{\vec{L}} \tag{A.16}$$

We can refer to the Coulombic Runge-Lenz vector as

$$\dot{\vec{A}_c} = \dot{\vec{p_c}} \times \vec{L} - \dot{\hat{r}} \tag{A.17}$$

For a $1/\vec{r}$ potential, $\dot{\vec{A}_c} = 0$. Therefore,

$$\dot{\vec{A}} = -\vec{F} \times \vec{L} + \vec{p} \times \dot{\vec{L}} \tag{A.18}$$

By applying Eq. (A.8) to $\vec{p} \times \dot{\vec{L}}$, we can write

$$\vec{p} \times \dot{\vec{L}} = \vec{p} \times (-\vec{r} \times \vec{F}) \tag{A.19}$$

Using the "BAC-CAB" rule for triple cross products,

$$\vec{A} \times (\vec{B} \times \vec{C}) = \vec{B} \cdot (\vec{A} \cdot \vec{C}) - \vec{C} \cdot (\vec{A} \cdot \vec{B}) \tag{A.20}$$

We can now write Eq. (A.19) as

$$\vec{p} \times \dot{\vec{L}} = F(\vec{p} \cdot \vec{r}) - \vec{r}(\vec{p} \cdot \vec{F}) \tag{A.21}$$

We now look to evaluate the time average of these two above terms.

$$\vec{p} \cdot \vec{r} = \frac{\mathrm{d}\vec{r}}{\mathrm{d}t} \cdot \vec{r} = \frac{1}{2} \frac{\mathrm{d}}{\mathrm{d}t} (\vec{r})^2 \tag{A.22}$$

The average over a whole period of an exact differential of a periodic function is zero, so Eq. (A.22) = 0. Thus,

$$\vec{p} \times \dot{\vec{L}} = -\vec{r}(\vec{p} \cdot \vec{F}) \tag{A.23}$$

This makes Eq. (A.18) become

$$\dot{\vec{A}} = -\vec{F} \times \vec{L} - \vec{r}(\vec{p} \cdot \vec{F}) \tag{A.24}$$

If we inspect the product $\vec{F} \times \vec{L}$,

$$\vec{F} \times \vec{L} = \vec{F} \times (\vec{r} \times \vec{p}) \tag{A.25}$$

which by the "BAC-CAB", Eq. (A.20), rule can be written as,

$$\vec{F} \times \vec{L} = \vec{r}(\vec{F} \cdot \vec{p}) - \vec{p}(\vec{F} \cdot \vec{r}) \tag{A.26}$$

This quantity can be shown to be equal to the negative derivative of $\vec{r}(\vec{r} \cdot \vec{F})$,

$$\vec{r}(\vec{F} \cdot \vec{p}) - \vec{p}(\vec{F} \cdot \vec{r}) = -\frac{\mathrm{d}}{\mathrm{d}t}\vec{r}(\vec{r} \cdot \vec{F}) \tag{A.27}$$

This exact differential also averages to zero. Therefore,

$$< \vec{r}(\vec{F} \cdot \vec{p}) >= - < \vec{p}(\vec{F} \cdot \vec{r}) > \tag{A.28}$$

If we substitute this into Eq. (A.26) we have the expression

$$\vec{F} \times \vec{L} = - < 2\vec{p}(\vec{F} \cdot \vec{r}) > \tag{A.29}$$

Finally applying this to Eq. (A.24) leads to an equation for $\dot{\vec{A}}$:

$$\dot{\vec{A}} = \frac{3}{2}(\vec{L} \times \vec{F}) \tag{A.30}$$

Eqs. (A.13) and (A.30) can be uncoupled and evaluated by differentiating one and substituting into the other equation. Differentiation of Eq. (A.30) yields the equation

$$\ddot{\vec{A}} = \frac{3}{2}((\dot{\vec{L}} \times \vec{F}) + (\dot{\vec{F}} \times \vec{L})) \tag{A.31}$$

Since we are investigating static fields, we can drop the second term from Eq. (A.31). Substituting Eq. (A.13) into Eq. (A.31) leads to

$$\ddot{\vec{A}} = \frac{3}{2}n^2((\vec{A} \times \vec{F}) \times \vec{F}) \tag{A.32}$$

Applying the fact that

$$\vec{A} \times \vec{B} = -(\vec{B} \times \vec{A}) \tag{A.33}$$

and the "BAC-CAB" rule, Eq. (A.20), we can then write

$$\ddot{\vec{A}} = -(\frac{3}{2}n)^2(\vec{A}(\vec{F} \cdot \vec{F}) - \vec{F}(\vec{F} \cdot \vec{A})) \tag{A.34}$$

If $\vec{F} = F_z$ then we have the set of equations

$$\ddot{A}_x = -(\frac{3}{2})^2 n^2 F^2 A_x \tag{A.35a}$$

$$\ddot{A}_y = -(\frac{3}{2})^2 n^2 F^2 A_y \tag{A.35b}$$

$$\ddot{A}_z = 0 \tag{A.35c}$$

These second-order differential equations can be solved by an equation of the form

$$A(t) = Ce^{i(\frac{3}{2}nFt)} \tag{A.36}$$

Setting our amplitudes as A_{x0} and A_{y0}, respectively, and $A_y(t = 0) = 0$, generates the equation:

$$A_x(t)^2 + A_y(t)^2 = A_{x0}^2 \cos^2(\omega_s t) + A_{y0}^2 \sin^2(\omega_s t) \tag{A.37}$$

where $\omega_s = 3/2nF$, the Stark frequency. A similar treatment of $\vec{L}$ leads to an equation analogous to Eq. (A.37).

Appendix B

Hamiltonian Scaling Derivation

This derivation is thanks to [32]. Our Coulombic Hamiltonian is the familiar

$$H = \frac{p^2}{2} - \frac{1}{r} \tag{B.1}$$

We can add a Stark field term in the z-direction to our Hamiltonian,

$$H = \frac{p^2}{2} - \frac{1}{r} + Fz \tag{B.2}$$

We now look to scale our position, r, and momentum, p, so that our Hamiltonian is independent of the applied Stark field. We can define our scaled variables as

$$r = F^{\alpha}\tilde{r} \tag{B.3a}$$

$$p = F^{\beta}\tilde{p} \tag{B.3b}$$

Our scaled Hamiltonian therefore becomes,

$$\tilde{H} = F^{2\beta}\frac{\tilde{p}^2}{2} - F^{-\alpha}\frac{1}{\tilde{r}} + F^{\alpha+1}\tilde{z} \tag{B.4}$$

Each term in our scaled Hamiltonian must have the same field dependence. Thus,

$$2\beta = -\alpha = \alpha + 1 \tag{B.5}$$

We can solve for α and β to be

$$\alpha = -\frac{1}{2} \tag{B.6a}$$

$$\beta = \frac{1}{4} \tag{B.6b}$$

We now have the scaling parameters:

$$r = F^{-1/2}\tilde{r} \tag{B.7a}$$

$$p = F^{1/4}\tilde{p} \tag{B.7b}$$

When these scaling variable are substituted into our Hamiltonian, Eq. (B.2), we can develop a scaled Hamiltonian relationship,

$$H = F^{1/2}\frac{\tilde{p}^2}{2} - F^{1/2}\frac{1}{\tilde{r}} + F(F^{-1/2})\tilde{z} \tag{B.8}$$

$$H = \tilde{H}F^{-1/2} \tag{B.9}$$

We can referred to the scaled energy of our scaled Hamiltonian as ϵ. From Eq. (B.9) leads the scaled energy relation

$$\epsilon = \frac{E}{\sqrt{F}} \tag{B.10}$$

Our scaled Hamiltonian is now completely independent of the external field.

Appendix C

Southwest Vacuum Devices

Cathode Installation

1. Place $C-14$ cathodes in cathode holder.
2. Using resistance welder, weld cathode leads onto cathode holder body.
3. For each source, weld one heater lead to cathode lead.
4. Weld nickel wire between un-welded heater leads(1)[1].
5. Weld nickel wire between cathode leads (2).
6. Assemble cathode holder together with base and extraction grid.
7. Weld external leads to nickel wire (1) and nickel wire (2) using nickel wire.
8. Install sweeper assembly onto source.

[1]To keep from confusion about heater leads, each heater has two leads. One lead of a heater shall be denoted (1), the other (2). The two heaters are wired in parallel.

9. Install source into vacuum chamber.

10. Pump chamber below 10^{-7} torr.

11. Check for electrical shorting between cathode and case, as well as continuity on cathode leads.

12. Apply 7.5 V to the cathode for three minutes.

13. Apply 12.5 V to the cathode for two minutes.

14. Apply 10 V to the cathode for thirty minutes. Put 125 V - 150 V bias on the cathode during this step.

15. Lower cathode voltage to $\sim$4 V and purge gas valve at a pressure no higher than 5×10^{-5} torr.

16. Run source at $\sim$9 V. Heaters should draw roughly 2.0 A.

Appendix D

Properties of Hydrogenic Ellipses

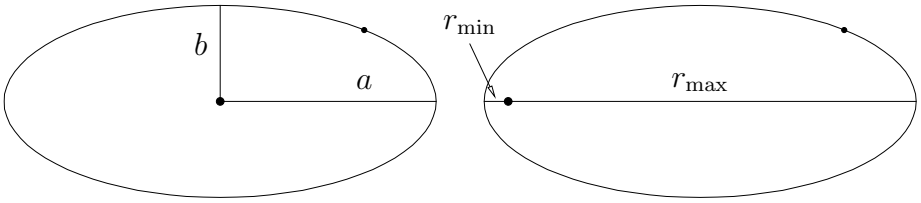

semimajor axis	$a = n^2$
semiminor axis	$b = nl$
orbital period	$\tau = 2\pi a^{3/2}$
orbital eccentricity	$\epsilon = \sqrt{1 - l^2/n^2}$
pericenter	$r_{min} = n^2(1 - \epsilon)$
apocenter	$r_{max} = n^2(1 + \epsilon)$

Appendix E

Pictures of the Portable Rydberg Generator

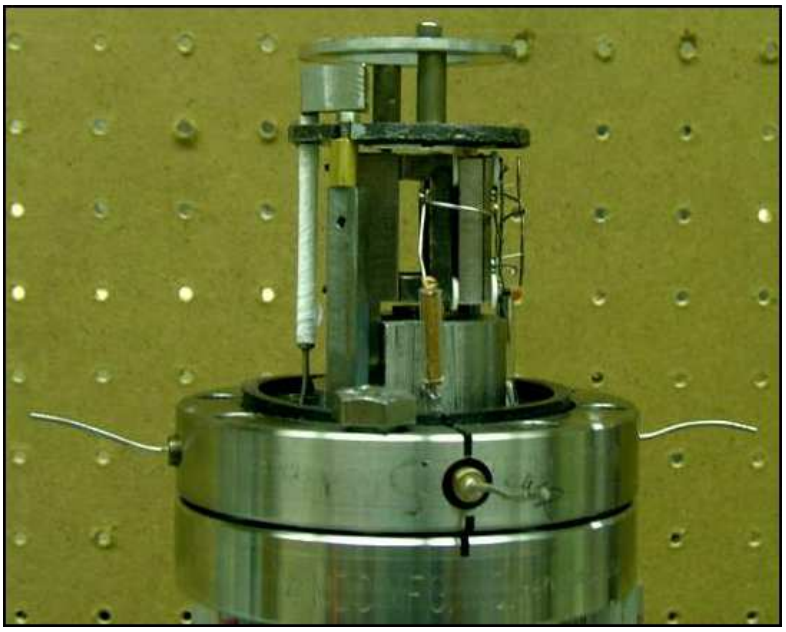

Figure E.1: View of metastable source from the Portable Rydberg Generator (Southwest Vacuum Devices cathodes)

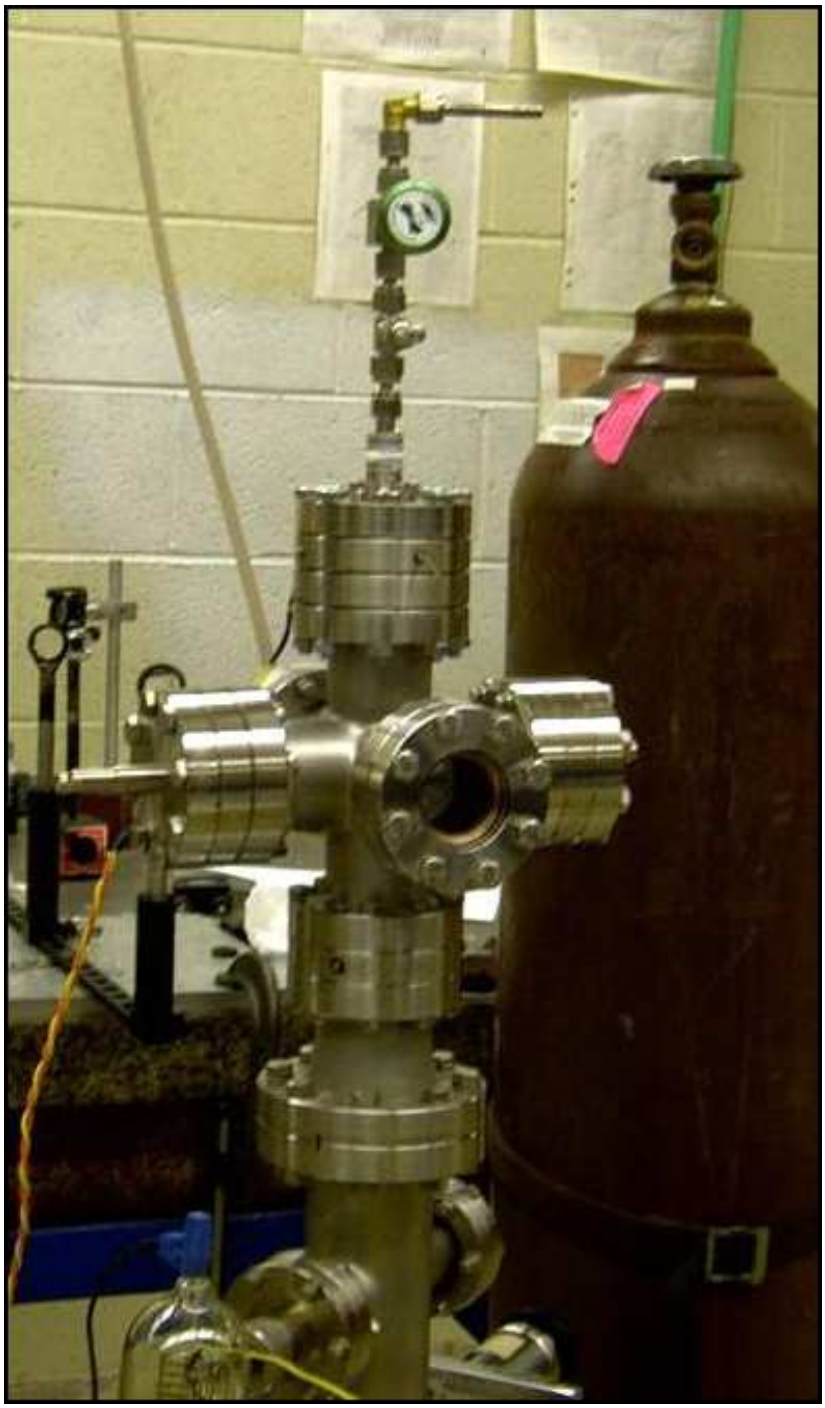

Figure E.2: Wide view of the Portable Rydberg Generator

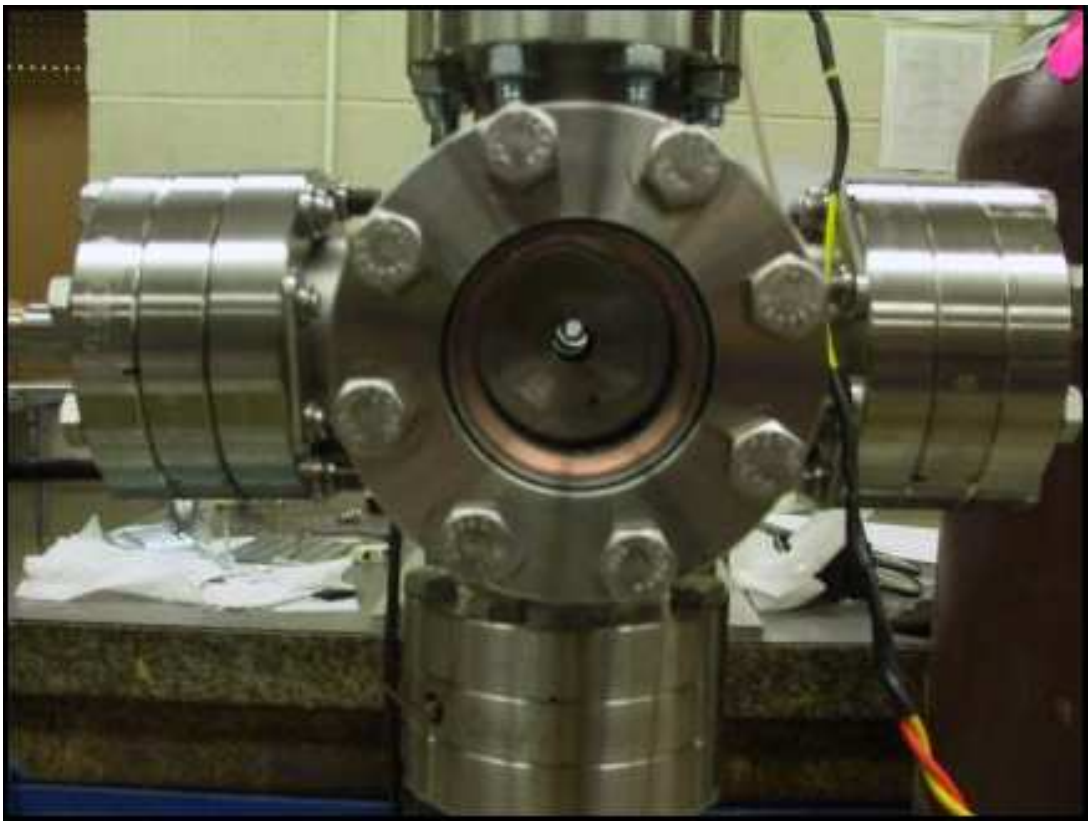

Figure E.3: Side view of the Portable Rydberg Generator

Bibliography

[1] N. Andersen, J. W. Gallagher, and I. V. Hertel. Collisional alignment and orientation of atomic outer shells: I. direct excitation by electron and atom impact. *Physics Reports*, 165:1, 1988.

[2] J. F. Baugh, D. A. Edmonds, P. T. Nellesen, C. E. Burkhardt, and J. J. Leventhal. Coherent states composed of Stark eigenfunctions of the hydrogen atom. *Am. J. Phys.*, 65:1097, 1997.

[3] R. J. Bell. *Introductory Fourier Transform Spectroscopy.* Academic Press, 1972.

[4] H. Bethe and E. Salpeter. *Quantum Mechanics of One- and Two-Electron Systems.* Plenum Publishing, 1977.

[5] J. B. Boffard, G. A. Piech, M. F. Gehrke, M. E. Lagus, L. W. Anderson, and C. C. Lin. Electron impact excitation out of the metastable levels of argon into the $3p^5 4p$ J = 3 level. *J. Phys. B: At. Mol. Opt. Phys.*, 29:L795, 1996.

[6] W. L. Borst. Excitation of metastable argon and helium atoms by electron impact. *Phys. Rev. Lett.*, 9:1195, 1974.

[7] J. Bretagne, G. Delouya, J. Godart, and V. Puech. High-energy electron distribution in an electron-beam-generated argon plasma. *J. Phys. D: Appl. Phys.*, 14:1225, 1981.

[8] Chemical Rubber Company. *CRC standard mathematical tables and formulae*. CRC Press, 1991.

[9] T. Clausen. *Quantum Chaos in the periodically driven Hydrogen Atom*. PhD thesis, Wesleyan University, 2002.

[10] E. U. Condon and G. H. Shortley. *The Theory of Atomic Spectra*. Cambridge University Press, 1959.

[11] D. Cullinan. Electric field effects on helium Rydberg atoms. Master's thesis, Wesleyan University, 1997.

[12] J. B. Delos, R. L. Waterland, and M. L. Du. Semiclassical interpretation of eigenvectors for excited atoms in external fields. *Phys. Rev. A*, 37:1185, 1988.

[13] M. L. Du and J. B. Delos. Effect of closed classical orbits on quantum spectra: Ionization of atoms in a magnetic field, I. physical picture and calculations. *Phys. Rev. A*, 38:1896, 1988.

[14] M. L. Du and J. B. Delos. Effect of closed classical orbits on quantum spectra: Ionization of atoms in a magnetic field. II. derivation of formulas. *Phys. Rev. A*, 38:1913, 1988.

[15] W. E. Ernst, T. P. Softley, and R. N. Zare. Stark-effect studies in xenon autoionizing Rydberg states using a tunable extreme-ultraviolet laser source. *Phys. Rev. A*, 37:4172, 1988.

[16] H. Flores-Rueda. *Stark Recurrence Spectroscopy of Rydberg Helium and Argon Atoms: The Covergence of Quantum and Classical Mechanics*. PhD thesis, Wesleyan University, 2002.

[17] A. P. French. *Vibrations and Waves*. W. W. Norton & Company, 1971.

[18] T. Gallagher. *Rydberg Atoms*. Cambridge University Press, 1994.

[19] J. Gao and J. B. Delos. Closed-orbit theory of oscillations in atomic photoabsorption cross sections in a strong electric field. II. derivation of formulas. *Phys. Rev. A*, 46:1455, 1992.

[20] J. Gao and J. B. Delos. Resonances and recurrences in the absorption spectrum of an atom in an electric field. *Phys. Rev. A*, 49:869, 1994.

[21] J. Gao, J. B. Delos, and M. Baruch. Closed-orbit theory of oscillations in atomic photoabsorption cross sections in a strong electric field. I. comparison between theory and experiments on hydrogen and sodium above threshold. *Phys. Rev. A*, 46:1449, 1992.

[22] H. Goldstein. *Classical Mechanics*. Addison-Wesley, 1980.

[23] D. Griffiths. *Introduction of Quantum Mechanics*. Prentice Hall, Inc., 1995.

[24] M. R. Haggerty and J. B. Delos. Recurrence spectroscopy in time-dependent fields. *Phys. Rev. A*, 61:053406, 2000.

[25] HeatWave Labs, Inc. TB-198 Standard Series Barium Tungsten Dispenser Cathodes. http://www.cathode.com/, 2002.

[26] T. P. Hezel, C. E. Burkhardt, M. Ciocca, L.-W. He, and J. J. Leventhal. Classical view of the properties of Rydberg atoms: Application of the correspondence principle. *Am. J. Phys.*, 60:329, 1992.

[27] T. P. Hezel, C. E. Burkhardt, M. Ciocca, and J. J. Leventhal. Classical view of the Stark effect in hydrogen atoms. *Am. J. Phys.*, 60:324, 1991.

[28] R. N. Il'in, B. I. Kikiani, V. A. Oparin, E. S. Solov'ev, and N. V. Fedorenko. Formation of highly excited hydrogen atoms by proton charge exchange in gases. *Sov. Phys. - JETP*, 20:835, 1965.

[29] J. D. Jackson and H. Schiff. Electron capture by protons passing through hydrogen. *Phys. Rev.*, 89:359, 1953.

[30] R. V. Jensen, H. Flores-Rueda, J. D. Wright, M. L. Keeler, and T. J. Morgan. Structure of the Stark recurrence spectrum. *Phys. Rev. A*, 62:053410, 2000.

[31] J. Kauppinen and J. Partanen. *Fourier Transforms in Spectroscopy.* Wiley-Vch, 2001.

[32] M. L. Keeler. *The Recurrence Spectroscopy of Helium.* PhD thesis, Wesleyan University, 1998.

[33] M. L. Keeler, H. Flores-Rueda, J. D. Wright, and T. J. Morgan. Scaled-energy spectroscopy of argon atoms in an electric field. *J. Phys. B*, 37:809, 2004.

[34] M. L. Keeler and T. J. Morgan. Scaled-energy spectroscopy of the Rydberg-Stark spectrum of helium: Influence of exchange on recurrence spectra. *Phys. Rev. Lett.*, 80:5726, 1998.

[35] M. L. Keeler and T. J. Morgan. Core-scattered combination orbits in the $m = 0$ Stark spectrum of helium. *Phys. Rev. A*, 59:4559, 1999.

[36] M. L. Keeler and T. J. Morgan. Behavior of non-classical recurrence amplitudes near closed orbit bifurcations in atoms. *Phys. Rev. A*, 69:012103, 2004.

[37] R. D. Knight and L. Wang. One-photon laser spectroscopy of the np and nf Rydberg series in xenon. *J. Opt. Soc. Am. B*, 2:1084, 1985.

[38] R. D. Knight and L. Wang. Stark structure in Rydberg states of xenon. *Phys. Rev. A*, 32:896, 1985.

[39] P. Labastie, F. Biraben, and E. Giacobino. Optogalvanic spectroscopy of the ns and nd Rydberg states of xenon. *J. Phys. B: At. Mol. Phys.*, 15:2595, 1982.

[40] L. D. Landau and E. M. Lifshitz. *Mechanics*. Butterworth-Heinemann, 1976.

[41] M. Mizushima. *Quantum Mechanics of Atomic Spectra and Atomic Structure*. W.A. Benjamin, 1970.

[42] A. J. Murray and P. Hammond. Laser probing of metastable atoms and molecules deflected by electron impact. *Phys. Rev. Lett.*, 82:4799, 1999.

[43] National Institute of Standards and Technology. NIST Atomic Spectra Database Levels Data Ar I. http://physics.nist.gov/cgi-bin/AtData/display.ksh?XXE1qArqIXXT2XXI, 2004.

[44] J. R. Oppenheimer. On the quantum theory of the capture of electrons. *Phys. Rev.*, 31:349, 1928.

[45] V. Puech and L. Torchin. Collision cross sections and electron swarm parameters in argon. *J. Phys. D: Appl. Phys.*, 19:2309, 1986.

[46] S. P. Renwick. *Quasi-Free Scattering in the Ionization and Destruction of Hydrogen and Helium Rydberg Atoms in Collision with Neutral Targets.* PhD thesis, Wesleyan University, 1991.

[47] J. R. Rubbmark, M. M. Kash, M. G. Littman, and D. Kleppner. Dynamical effects at avoided level crossing: A study of the Landau-Zener effect using Rydberg atoms. *Phys. Rev. A*, 23:3107, 1981.

[48] J. A. Shaw, J. B. Delos, M. Courtney, and D. Kleppner. Recurrences associated with a classical orbit in the node of a quantum wave function. *Phys. Rev. A*, 52:3695, 1995.

[49] H. J. Silverstone. Perturbation theory of the Stark effect in hydrogen to arbitrarily high order. *Phys. Rev. A*, 18:1853, 1978.

[50] R. F. Stebbings and F. B. Dunning. *Rydberg states of atoms and molecules.* Cambridge University Press, 1983.

[51] R. F. Stebbings, C. J. Latimer, W. P. West, F. B. Dunning, and T. B. Cook. Studies of xenon atoms in high Rydberg states. *Phys. Rev. A*, 12:1453, 1975.

[52] O. Tommasi, G. Bertuccelli, M. Francesconi, F. Giammanco, D. Romanini, and F. Strumia. A high-density collimated metastable he beam with population inversion. *J. Phys. D: Appl. Phys.*, 25:1408, 1992.

[53] I. Velchev, W. Hogervorst, and W. Ubachs. Precision VUV spectroscopy of Ar I at 105 nm. *J. Phys. B: At. Mol. Opt. Phys.*, 32:L511, 1999.

[54] L. Wang and R. D. Knight. Two-photon laser spectroscopy of the ns′ and nd′ autoionizing Rydberg series in xenon. *Phys. Rev. A*, 34:3902, 1986.

[55] J. B. M. Warntjes, C. Nicole, F. Rosca-Pruna, I. Sluimer, and M. J. J. Vrakking. Two-channel competition of autoionizing Rydberg states in an electric field. *Phys. Rev. A*, 63:053403, 2001.

[56] W. P. West, G. W. Foltz, F. B. Dunning, C. J. Latimer, and R. F. Stebbings. Absolute measurements of collisional ionization of xenon atoms in well-defined high Rydberg states. *Phys. Rev. Lett.*, 36:854, 1975.

[57] M. L. Zimmerman, M. G. Littman, M. M. Kash, and D. Kleppner. Stark structure of the Rydberg states of alkali-metal atoms. *Phys. Rev. A*, 20:2251, 1979.

Index

action, 26
    principle of least action, 26
aluminum, 38
angular momentum, 10, 11, 15, 48
argon, 1, 20, 37, 38, 40, 41, 43, 45
atomic units, 12
avoided crossings, 20

Bethe, H., 17, 35
Bohr, N., 9, 10
    Bohr model, 9, 16

Channeltron, 30, 46
charge transfer, 30, 32, 34–36
closed orbit theory, 20, 26–28
Colutron, 32
Coulomb potential, 8, 11, 13, 15, 16, 19

de Broglie
    formula, 10
    wavelength, 10
Delos, J. B., 27
dipole
    energy, 14
    moment, 11, 13
    selection rules, 33, 34
    torque, 49
Dirac delta function, 25
Du, M. L., 27
Dunning, F. B., 20

electric quantum number, 17
electron orbital radius, 10
electron impact, 30, 32, 34, 36, 43, 45–47
electron orbital radius, 10
ellipse, 13, 15
    apocenter, 57
    eccentricity, 13, 14, 57
    focus, 13
    orbit, 13
    orbital period, 57
    pericenter, 13, 57

precession, 15
semimajor axis, 15, 57
semiminor axis, 15, 57
end-cup, 30, 31, 40, 43, 44
energy defect, 36
Ernst, W. E., 20

fast-atom beam, 29, 30, 36, 46
Flores-Rueda, H., 28
Fourier transform, 24–27
FFT, 26

Gao, J., 27

Hamilton's equations, 14, 48
Hamiltonian, 17, 22, 23, 48, 49, 53, 54
HeatWave Labs, 37, 38, 42, 44, 45
helium, 20, 36, 37
Hezel, T. P., 14, 17, 48
hydrogen, 9, 11, 13–17, 19, 33, 34
molecular, 47
zero field, 16

Il'in, R. N., 36

Jackson, J. D., 36

Keeler, M. L., 22, 24, 27–29, 36, 38
Keplerian orbit, 9–11
Knight, R. D., 20

Landau, L. D., 13
Lifshitz, E. M., 13

MDC, 29
metastable, 1, 30, 32, 34–38, 41–46
Morgan, T. J., 47
Morgan Lab, 1, 20, 24, 27, 29, 36, 47

Nd:YAG laser, 23
nickel, 40, 55
work function, 40

Oppenheimer, J. R., 36

parabolic coordinates, 17, 18, 20, 28, 49
perturbation theory, 18
first order, 18, 19
second order, 18, 19
polar coordinates, 11
potassium, 36
PRG, 1, 29, 30, 32, 38, 39, 43, 58–60

quantum chaos, 8
quantum defect, 20

Runge-Lenz vector, 13, 14, 17, 50
Russell-Saunders approximation, 35
Rydberg atom, 1, 8, 9, 20, 21, 30, 32, 33, 46
Rydberg formula, 11, 12, 19, 33

Salpeter, E., 17, 35
scaled action, 26
scaled energy, 23, 24, 54
scaling variables, 23
Schrödinger equation, 16
Silverstone, H. J., 18
sodium, 21, 36
Softley, T. P., 20
Southwest Vacuum Devices, 38–41, 43, 44, 58
spectroscopy, 23
  absorption, 21–24, 26, 27, 46
  laser, 29
  optogalvanic, 21
  recurrence, 1, 8, 21, 22, 26, 27, 36, 47
spherical coordinates, 16, 17
spin-orbit coupling, 35
spontaneous emission, 34
Stark
  field, 1, 8, 9, 11, 15, 17, 21, 30, 46, 49, 53
  frequency, 15, 52
  shift, 19
Stebbings, R. F., 20
sweepers, 30, 32, 33, 40, 44

Tommasi, O., 37

Wang, Liang-guo, 20
Warntjes, J. B. M., 21
Wright, J. D., 30

xenon, 20, 21, 35, 37, 38, 40, 46, 47

Zare, R. N., 20